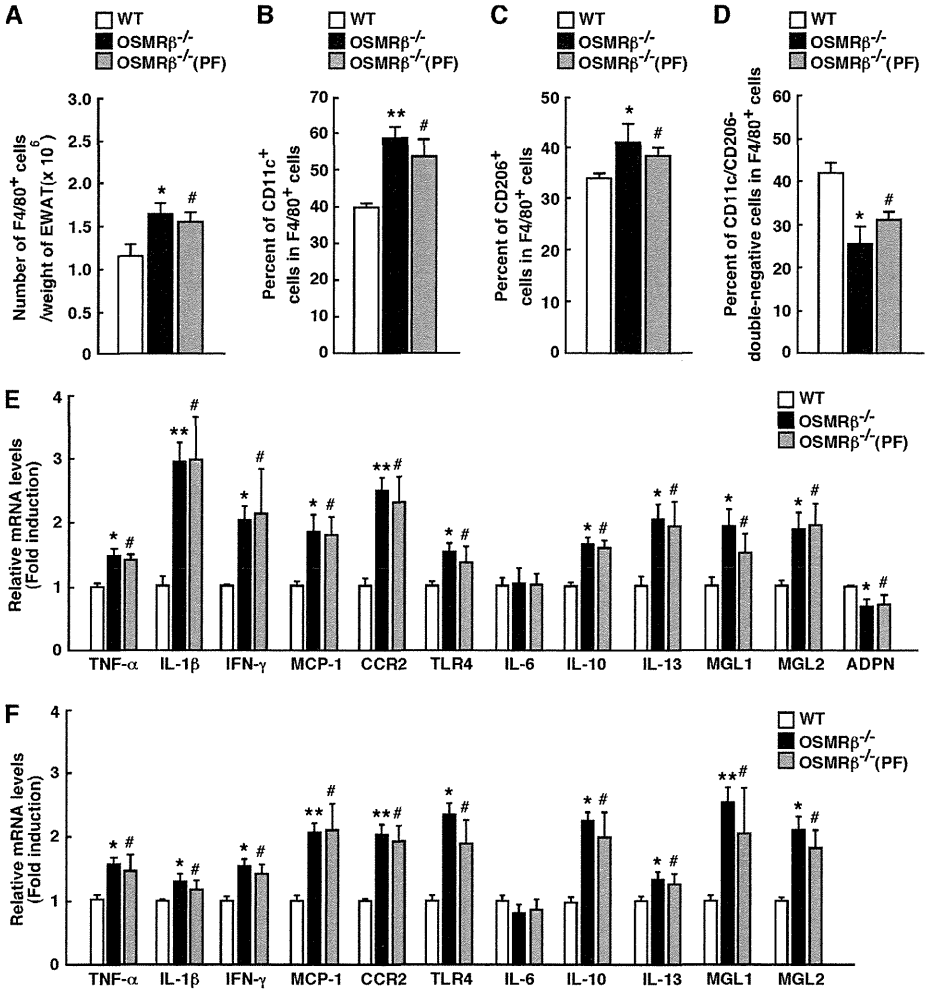

FIGURE 6. **Adipose tissue inflammation in WT and OSMR$\beta^{-/-}$ mice at 8 weeks on the HFD.** The mice (8 weeks old) were fed an HFD for 8 weeks. *A*, total number of F4/80-positive cells per weights of adipose tissue in WT, OSMR$\beta^{-/-}$, and OSMR$\beta^{-/-}$(PF) mice ($n = 6$). *EWAT*, epididymal white adipose tissue. *B* and *C*, the percentages of CD11c-positive cells (*B*) and CD206-positive cells (*C*) among the F4/80-positive cells in WT, OSMR$\beta^{-/-}$, and OSMR$\beta^{-/-}$(PF) mice. *D*, the percentages of CD11c/CD206-double-negative cells among the F4/80-positive cells in WT, OSMR$\beta^{-/-}$, and OSMR$\beta^{-/-}$(PF) mice. *E* and *F*, the mRNA expression levels of inflammatory and anti-inflammatory markers (TNF-α, IL-1β, IFN-γ, CCR2, MCP-1, TLR4, IL-6, MGL1, MGL2, IL-10, IL-13, and adiponectin) in the adipose tissue (*E*) and SVF (*F*) of WT, OSMR$\beta^{-/-}$, and OSMR$\beta^{-/-}$(PF) mice ($n = 6$). *ADPN*, adiponectin. The data represent the mean ± S.E. *, $p < 0.05$; **, $p < 0.01$ WT *versus* OSMRβ−/− mice; #, $p < 0.05$ WT *versus* OSMR$\beta^{-/-}$(PF) mice, Student's *t* test.

ob/*ob* mice compared with those observed in *ob*/*ob* mice with vehicle injection (Fig. 8, *A* and *B*). Both the blood glucose and serum insulin levels were also reduced by the treatment with OSM in the fasted state (Fig. 8, *C* and *D*). Treatment of *ob*/*ob* mice with OSM improved their glucose intolerance in an ipGTT (Fig. 8, *E* and *F*). The OSM-treated *ob*/*ob* mice were more sensitive to insulin, as measured by the ITT (Fig. 8, *G* and *H*). Therefore, OSM improves glucose intolerance and insulin resistance in *ob*/*ob* mice. In addition, the number of F4/80-positive macrophages per weight of adipose tissue was decreased in the adipose tissue by the treatment of OSM (Fig. 8*I*). The percentage of CD11c-positive M1-type macrophages was reduced, whereas the percentage of CD206-positive M2-type macrophages was increased in OSM-treated *ob*/*ob* mice (Fig. 8, *J* and *K*). In addition, OSM increased the expression of IL-10, IL-13, MGL1, and MGL2 in the adipose tissue of *ob*/*ob* mice (Fig. 8*L*). Furthermore, the Oil Red O staining revealed that lipid accumulation was reduced by the treatment of OSM in the liver of *ob*/*ob* mice (Fig. 8*M*). In contrast, the PAS staining showed that there were more glycogen granules in the hepatocytes of *ob*/*ob* mice treated with OSM compared with those observed in *ob*/*ob* mice with vehicle injection (Fig. 8*M*). In addition, the total cholesterol and triglyceride levels in the liver of *ob*/*ob* mice were decreased by the treatment of OSM (Fig. 8, *N* and *O*).

Direct Effects of OSM on the Liver of Genetically Obese ob/ob Mice—Consistent with the data in Fig. 1, *C* and *D*, the expression of OSMRβ was increased in the liver of the obese mice (Fig. 9, *A* and *B*). To investigate the direct effects of OSM on the liver of obese mice, we injected *ob*/*ob* mice with OSM intraportally. The activation of STAT3 was observed in the liver at 15 min after the intraportal injection of OSM (Fig. 9*C*). Furthermore, the expressions of both ACSL3 and ACSL5 were increased at 60 and 120 min after the intraportal injection of OSM (Fig. 9*D*). In addition, OSM decreased the expression of FAS in the liver of *ob*/*ob* mice (Fig. 9*D*). These results suggest that OSM directly acts on the liver in obese mice.

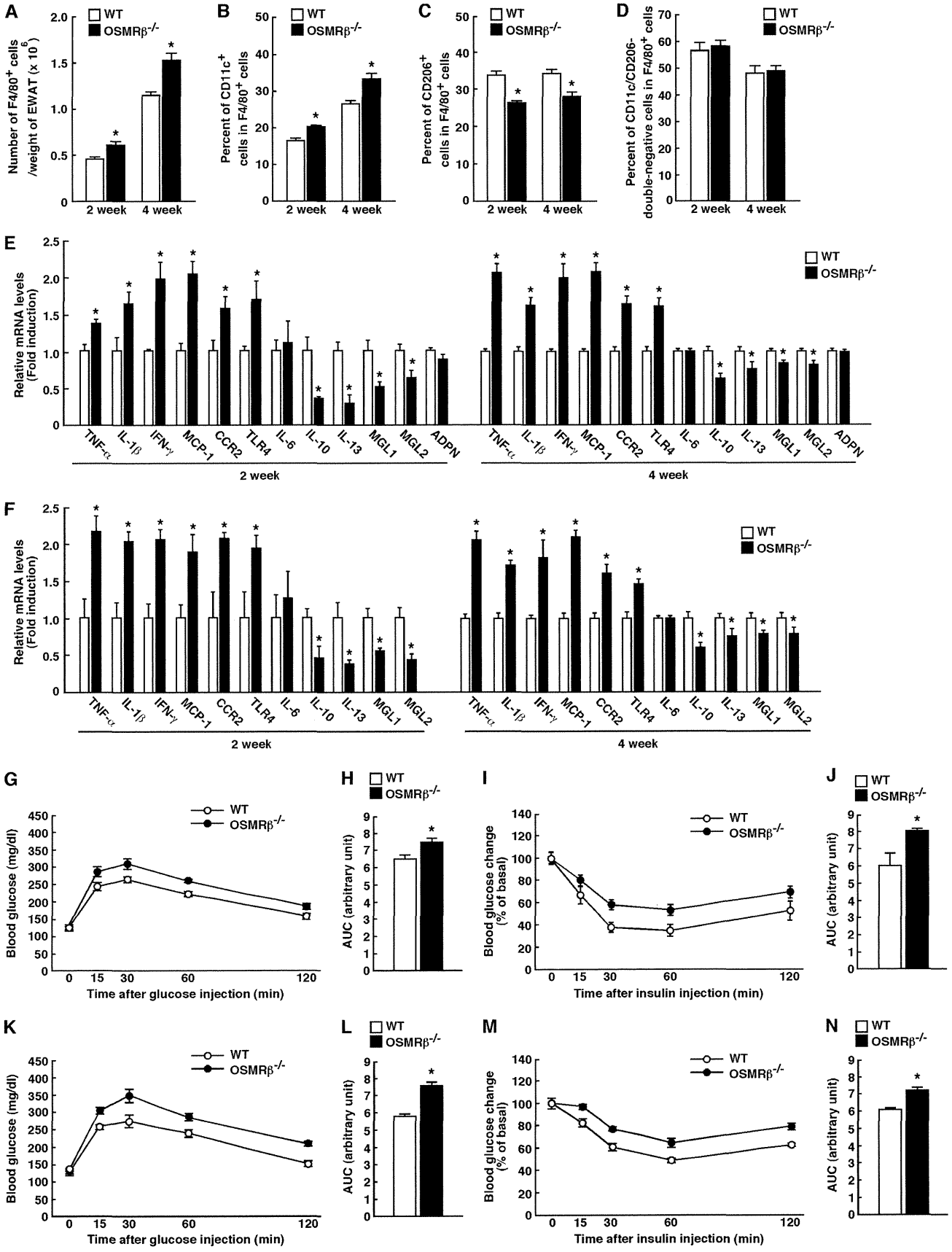
A
Number of F4/80+ cells /weight of EWAT (x 10^6)
WT
OSMRβ-/-
2 week
4 week
B
Percent of CD11c+ cells in F4/80+ cells
C
Percent of CD206+ cells in F4/80+ cells
D
Percent of CD11c/CD206-double-negative cells in F4/80+ cells
E
Relative mRNA levels (Fold induction)
TNF-α
IL-1β
IFN-γ
MCP-1
CCR2
TLR4
IL-6
IL-10
IL-13
MGL1
MGL2
ADPN
2 week
4 week
F
G
Blood glucose (mg/dl)
Time after glucose injection (min)
H
AUC (arbitrary unit)
I
Blood glucose change (% of basal)
Time after insulin injection (min)
J
K
L
M
N

DISCUSSION

OSM is a member of the IL-6 family of cytokines and plays a role in a variety of physiological functions, including hematopoiesis, the development of neurons, and the modulation of inflammatory responses (20, 30–32). Some members of this family, such as IL-6, ciliary neurotrophic factor, and cardiotrophin-1, are known to be associated with the development of obesity and insulin resistance (33–35). Although we have demonstrated the expression of OSMRβ in ATMs and its association with systemic insulin resistance in a previous report (21), the role of OSM signaling in the development of obesity and related metabolic disorders remains unclear. In the present study we first examined the expression of OSMRβ in the various tissues of both DIO and genetically obese *ob*/*ob* mice. The expression of OSMRβ was increased in the adipose tissue and liver of in these obese mice compared with their control mice. In the adipose tissue, OSMRβ was increased in the SVF, especially in the F4/80-positive ATMs, in both models of obese mice. These results suggest that OSM signaling is strongly associated with the pathogenesis of obesity and related metabolic disorders.

Next, we analyzed metabolic parameters in OSMR$\beta^{-/-}$ mice fed the HFD. Strikingly, feeding an HFD for 8 weeks resulted in more severe obesity in OSMR$\beta^{-/-}$ mice than in WT mice. Hyperglycemia, hyperinsulinemia, insulin resistance, adipose tissue inflammation, and hepatic steatosis were exacerbated in OSMR$\beta^{-/-}$ mice under HFD conditions. In addition, OSM improved adipose tissue inflammation, insulin resistance, and hepatic steatosis of *ob*/*ob* mice. These results suggest that OSM signaling has suppressive effects on the deterioration of obesity and related metabolic disorders.

Obesity is an important cause of the development of metabolic disorders (2). In the past decade, it has been widely accepted that HFD leads to obesity that causes chronic low-grade inflammation followed by insulin resistance (2). Then, insulin resistance leads to hyperinsulinemia and β cell failure successively, resulting in various metabolic disorders, including type 2 diabetes and hepatic steatosis. Therefore, there is the possibility that the deterioration of metabolic disorders noted in OSMR$\beta^{-/-}$ mice was due to the increase in fat mass. However, the pair-feeding study revealed that none of the metabolic disorders observed in OSMR$\beta^{-/-}$ mice fed the HFD, including adipose tissue inflammation, insulin resistance, and hepatic steatosis, was affected by the decrease in food intake and body weight in OSMR$\beta^{-/-}$ mice pair-fed with WT mice. These results suggest that the effects of OSM signaling on the deterioration of metabolic disorders associated with diet-induced obesity are independent of changes in food intake and body weight. In addition, the deterioration of adipose tissue inflammation, hyperinsulinemia, insulin resistance, and glucose intolerance were already observed in OSMR$\beta^{-/-}$ mice at 2 weeks on the HFD, when there was no difference in body weight between WT and OSMR$\beta^{-/-}$ mice. Recently, Mehran *et al.* (36) have proposed a novel model of obesity and type 2 diabetes distinct from the widely accepted model in which hyperinsulinemia is upstream of obesity. Thus, the relationships between obesity, insulin resistance, and hyperinsulinemia need to be revisited, and we are considering OSMR$\beta^{-/-}$ mice as a unique mouse model of metabolic diseases.

Under conditions of obesity, inflammatory cytokines, such as TNF-α, IL-1β, and IFN-γ, are primarily secreted from M1-type ATMs, which induces insulin resistance (7–11, 37, 38). In contrast, an anti-inflammatory cytokine, IL-10, is produced by M2-type ATMs, which suppresses insulin resistance (7, 12, 13). In our previous study OSM signaling was found to have a suppressive effect on adipose tissue inflammation due to the polarization of the macrophage phenotype to the M2-type under normal dietary conditions (21). In the present study feeding an HFD induced the expression of OSMRβ in ATMs, suggesting the important role of OSM in the development of adipose tissue inflammation under conditions of obesity. As expected, OSMR$\beta^{-/-}$ mice, in which OSM signaling is deleted, exhibited increases in both the number of M1-type ATMs and expression levels of inflammatory cytokines in the adipose tissue when fed the HFD for 8 weeks. At this stage, insulin resistance was exacerbated in OSMR$\beta^{-/-}$ mice compared with that observed in WT mice, suggesting that adipose tissue inflammation enhanced by M1-type ATMs may contribute to the exacerbation of insulin resistance in OSMR$\beta^{-/-}$ mice. Recently, it has been reported that these inflammatory and anti-inflammatory cytokines are produced by other types of cells, such as regulatory T cells and CD8-positive T cells, and play important roles in the development of obesity-related metabolic disorders (5, 39). We cannot exclude the possibility that the changes in cytokine production profiles result from the other cells except for ATMs in OSMR$\beta^{-/-}$ mice. However, it is possible that ATMs are responsible for the inflammatory cytokine production profiles in OSMR$\beta^{-/-}$ mice directly because OSMRβ was exclusively expressed in F4/80-positive macrophages on adipose tissues under obese conditions.

On the other hand, the number of M2-type macrophages and the expression level of IL-10 were also increased in the adipose tissue of OSMR$\beta^{-/-}$ mice compared with those observed in WT mice. As the inflammatory responses driven by M1-type macrophages are often counteracted by protective mechanisms operated by M2-type macrophages (40), we analyzed the degree of adipose tissue inflammation and insulin resistance in OSMR$\beta^{-/-}$ mice at an early stage of HFD. At 4 weeks on the HFD, the number of M2-type macrophages and the expression levels of anti-inflammatory cytokines were low in the adipose tissue of OSMR$\beta^{-/-}$ mice compared with that observed in WT mice, whereas OSMR$\beta^{-/-}$ mice exhibited an increased num-

FIGURE 7. **Adipose tissue inflammation and glucose metabolism in WT and OSMR$\beta^{-/-}$ mice at 2 and 4 weeks on the HFD.** *A*, total number of F4/80-positive cells per weights of adipose tissue in WT and OSMR$\beta^{-/-}$ mice ($n = 6$). *B* and *C*, the percentages of CD11c-positive cells (*B*) and CD206-positive cells (*C*) among the F4/80-positive cells in WT and OSMR$\beta^{-/-}$ mice. *D*, the percentages of CD11c/CD206-double-negative cells among the F4/80-positive cells in WT and OSMR$\beta^{-/-}$ mice. *E* and *F*, the mRNA expression levels of inflammatory and anti-inflammatory markers (TNF-α, IL-1β, IFN-γ, CCR2, MCP-1, TLR4, IL-6, MGL1, MGL2, IL-10, IL-13, and adiponectin) in the adipose tissue (*E*) and SVF (*F*) of WT and OSMR$\beta^{-/-}$ mice ($n = 6$). *G–N*, the results of the ipGTTs (*G* and *K*) and ITTs (*I* and *M*) in WT and OSMR$\beta^{-/-}$ mice at 2 weeks (*G–J*) and 4 weeks (*K–N*) on the HFD ($n = 6$). The AUC for blood glucose on the ipGTTs (*H* and *L*) and ITTs (*J* and *N*) was shown. *ADPN*, adiponectin. The data represent the mean ± S.E. *, $p < 0.05$; **, $p < 0.01$ WT *versus* OSMR$\beta^{-/-}$ mice, Student's *t* test.

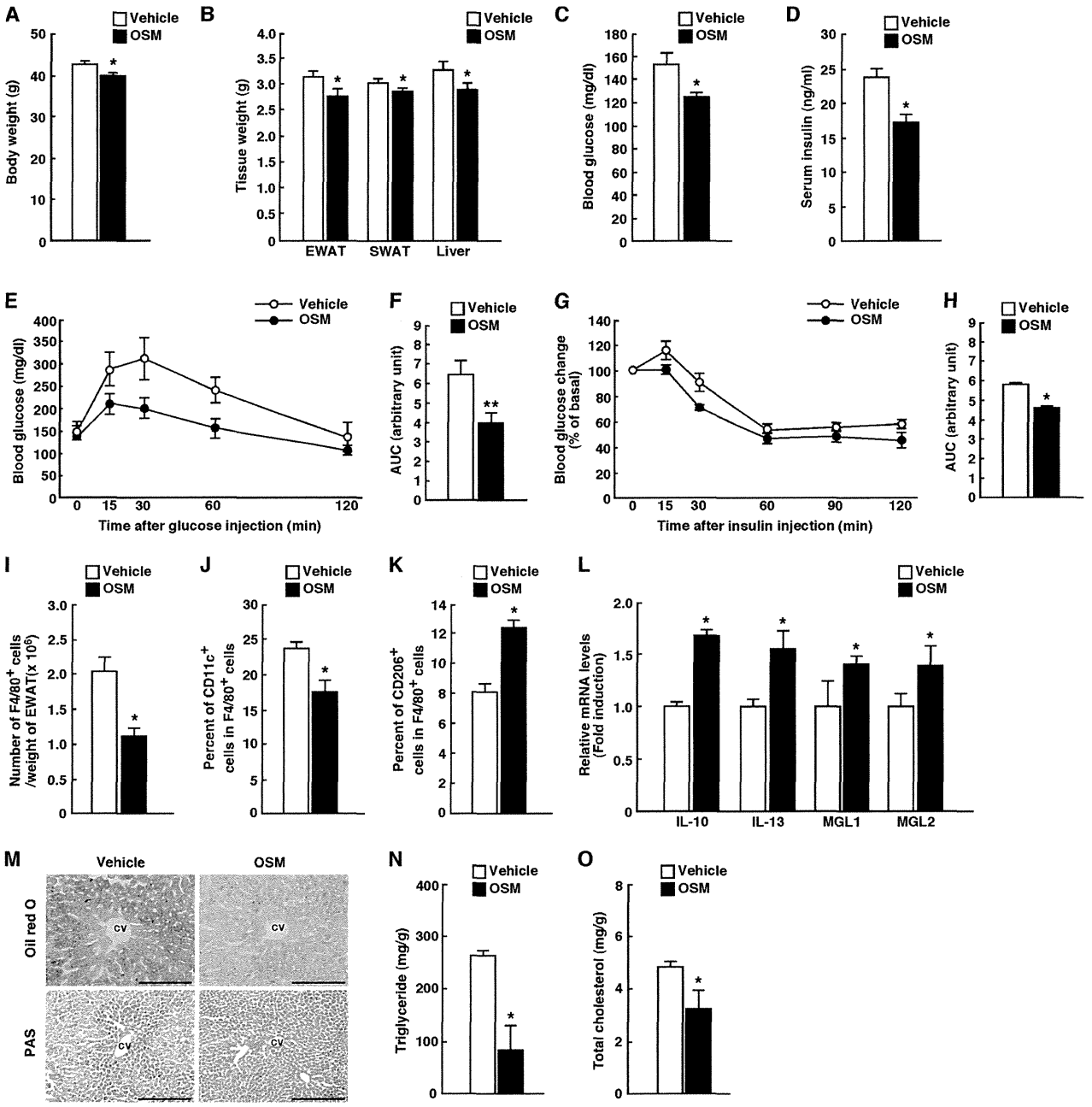

FIGURE 8. **The effects of OSM on glucose metabolism, adipose tissue inflammation, and hepatic steatosis in *ob/ob* mice.** *ob/ob* mice were injected intraperitoneally with either vehicle or recombinant mouse OSM (12.5 ng/g of body weight) twice a day for 7 days. *A*, the body weights in vehicle- and OSM-treated *ob/ob* mice ($n = 6$). *B*, the tissue weights in vehicle- and OSM-treated *ob/ob* mice ($n = 6$). *EWAT*, epididymal white adipose tissue; *SWAT*, subcutaneous white adipose tissue. *C* and *D*, blood glucose (*C*) and serum insulin (*D*) levels in vehicle- and OSM-treated *ob/ob* mice in the fasted states ($n = 6$). In the fasted states, mice were fasted overnight before the experiments. *E–H*, the results of the ipGTTs (*E*) and ITTs (*G*) in vehicle- and OSM-treated *ob/ob* mice ($n = 6$). The AUC for blood glucose on the ipGTTs (*F*) and ITTs (*H*) is shown. For ipGTTs, mice were fasted for 16 h and intraperitoneally injected with D-glucose (0.5 g/kg of body weight). For ITTs, mice were fasted for 4 h and intraperitoneally injected with insulin (5 unit/kg of body weight). *I*, total number of F4/80-positive cells per weights of adipose tissue in vehicle- and OSM-treated *ob/ob* mice ($n = 6$). *J* and *K*, the percentages of CD11c-positive cells (*J*) and CD206-positive cells (*K*) among the F4/80-positive cells in vehicle- and OSM-treated *ob/ob* mice. *L*, the mRNA expression levels of anti-inflammatory markers (IL-10, IL-13, MGL1, and MGL2) in the adipose tissue of vehicle- and OSM-treated *ob/ob* mice ($n = 6$). *M*, Oil Red O and PAS staining of the livers of vehicle- and OSM-treated *ob/ob* mice. *CV*, central vein. *Scale bar* = 100 μm. *N* and *O*, the content of triglycerides (*N*) and total cholesterol (*O*) in the livers of vehicle- and OSM-treated *ob/ob* mice in the fed state ($n = 6$). In the fed state, mice were fasted for 4 h before the experiments to eliminate the feeding effects on lipid metabolism. The data represent the mean ± S.E. *, $p < 0.05$; **, $p < 0.01$ vehicle *versus* OSM, Student's *t* test.

ber of M1-type ATMs, high expression levels of inflammatory cytokines, and severe insulin resistance. Therefore, the increased anti-inflammatory responses observed in OSMR$\beta^{-/-}$ mice at 8 weeks on the HFD may have occurred to counteract the excessive inflammation induced by the larger number of M1-type ATMs and the up-regulation of inflammatory cytokines in the adipose tissue. In addition, an increased total number of ATMs, the polarization of ATMs to M1-type,

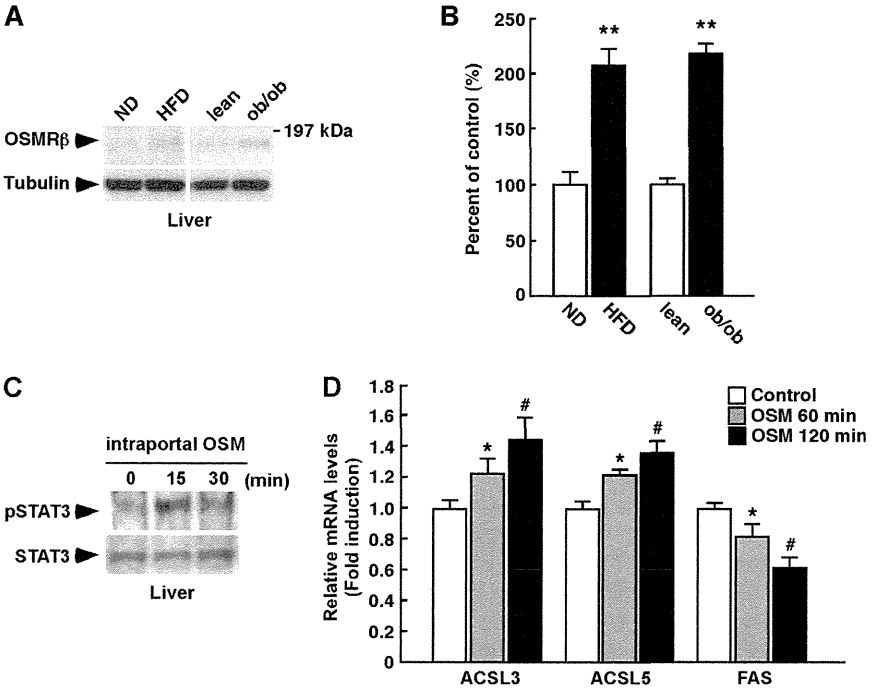

FIGURE 9. **The direct effects of OSM on liver lipid metabolism in *ob/ob* mice.** *ob/ob* mice were injected intraportally with either vehicle or recombinant mouse OSM (12.5 ng/g of body weight) and maintained for 60 and 120 min. *A*, Western blot analysis of OSMRβ in the liver in the WT mice fed a normal diet (*ND*) or an HFD and the lean and *ob/ob* mice ($n = 6$). The apparent molecular masses are indicated on the *right*. *B*, a quantitative analysis of the protein expression of OSMRβ in the liver ($n = 6$). *C*, activation of STAT3 in the liver by the intraportal injection of OSM in *ob/ob* mice. *D*, the mRNA expression levels of genes related to lipolysis (*ACSL3* and *ACSL5*) and lipogenesis (*FAS*) in the liver of vehicle- and OSM-injected *ob/ob* mice ($n = 6$). The data represent the mean ± S.E. **, $p < 0.01$ normal diet (*ND*) *versus* HFD or lean *versus ob/ob* (*B*); *, $p < 0.05$ vehicle *versus* OSM 60 min; #, $p < 0.05$ vehicle *versus* OSM 120 min; Student's *t* test.

and inflammatory cytokine production profiles were already observed in OSMR$\beta^{-/-}$ mice at 2 weeks on the HFD. At this stage, hyperinsulinemia, glucose intolerance, and insulin resistance in OSMR$\beta^{-/-}$ mice were more severe than those in WT mice despite no differences in body weight between two genotypes, suggesting that the deterioration of these metabolic disturbances in OSMR$\beta^{-/-}$ mice occurs independent of the increase in body weight.

Obesity-induced insulin resistance causes serious metabolic disorders, including cardiovascular disease and hepatic steatosis (1, 41). Hepatic steatosis, in particular, is a predisposing factor for non-alcoholic steatohepatitis, which often progresses to liver cirrhosis and hepatocellular carcinoma (42). In the present study, OSMR$\beta^{-/-}$ mice fed an HFD for 8 weeks exhibited severe hepatic steatosis compared with that observed in WT mice. The expression levels of the transcription factor, SREBF-1, and its target genes, FAS and SCD-1, were also increased in the liver of OSMR$\beta^{-/-}$ mice. As FAS and SCD-1 promote fatty acid synthesis in the liver, increased *de novo* lipogenesis in the liver may result in the deterioration of hepatic steatosis in OSMR$\beta^{-/-}$ mice. Furthermore, insulin stimulates *de novo* lipogenesis by increasing the expression of SREBF-1 (43). We observed that the serum concentration of insulin was high in OSMR$\beta^{-/-}$ mice compared with those observed in WT mice, suggesting that the up-regulation of insulin induces an increased expression of SREBF-1 in OSMR$\beta^{-/-}$ mice. Therefore, hepatic steatosis is likely exacerbated in HFD-fed OSMR$\beta^{-/-}$ mice due to the promotion of hepatic lipogenesis.

It has been long accepted that insulin resistance and hepatic steatosis are mutually related in a "vicious cycle" (41). On the other hand, some investigators have recently reported the dissociation of hepatic steatosis from insulin resistance (44); insulin resistance without hepatic steatosis (with hypotriglycemia) has been observed in liver-specific insulin receptor knock-out mice (45, 46) and the liver-specific deletion of phosphatase and tensin homolog has been found to improve systemic insulin resistance associated with enhanced hepatic steatosis (47). Hence, hepatic steatosis is not always related to insulin resistance. To address this issue, Brown and Goldstein (48) proposed the concept of "selective insulin resistance." When insulin signaling is completely blunted in the liver, hepatic gluconeogenesis is promoted, and hepatic lipogenesis is inhibited. However, when some steps of insulin signaling only required for the suppression of hepatic gluconeogenesis are blunted in liver, the remaining intact mechanisms of insulin signaling drive hepatic lipogenesis. In the present study, we demonstrated that the activation of FOXO1 due to stimulation with insulin, which suppresses the gluconeogenetic actions of insulin, was inhibited in the liver of OSMR$\beta^{-/-}$ mice compared with that observed in WT mice. On the other hand, the phosphorylation of S6K after stimulation with insulin, which promotes *de novo* lipogenesis, remained intact in the liver of OSMR$\beta^{-/-}$ mice. As the degree of hyperinsulinemia was much more severe in OSMR$\beta^{-/-}$ mice than in WT mice, selective insulin resistance may contribute to the progression of hepatic steatosis in OSMR$\beta^{-/-}$ mice. Of course, we cannot rule out the possibility that other pathways may induce *de novo* lipogenesis in the liver, including glucose-induced carbohydrate response element-binding protein activation (49) and/or cholesterol-induced liver X receptor activation (50).

Alternatively, the cause of severe hepatic steatosis in OSMR$\beta^{-/-}$ mice is the lack of direct effects of OSM on the liver. In the present study, we observed that OSMRβ was up-regulated in the liver of obese mice. To test the direct effects of OSM on the liver, we injected OSM intraportally in *ob/ob* mice. A signal molecule for the downstream of OSMRβ, STAT3, was activated in the liver by the intraportal injection of OSM. Zhou *et al.* (51) have reported that the expression of ACSL3 and ACSL5, which promote lipolysis in the liver, is increased by OSM in HepG2 cells. In the present study, the intraportal injection of OSM increased the expression of ACSL3 and ACSL5 in the liver of obese mice. In addition, OSM decreased the expression of FAS in the liver. Thus, OSM may directly increase lipolysis and suppresses lipogenesis in the liver of obese mice.

In conclusion, OSMR$\beta^{-/-}$ mice exhibited severe obesity, adipose tissue inflammation, insulin resistance, and hepatic steatosis under HFD conditions. In addition, OSM improved adipose tissue inflammation, insulin resistance, and hepatic steatosis in genetically obese *ob/ob* mice. Our results strongly suggest that OSMRβ is required to protect against the development of obesity and related metabolic disorders. Therefore, OSM signaling is a potential novel therapeutic target in patients with metabolic syndrome, including obesity, insulin resistance, and hepatic steatosis.

REFERENCES

1. Bornfeldt, K. E., and Tabas, I. (2011) Insulin resistance, hyperglycemia, and atherosclerosis. *Cell Metab.* **14,** 575–585
2. Osborn, O., and Olefsky, J. M. (2012) The cellular and signaling networks linking the immune system and metabolism in disease. *Nat. Med.* **18,** 363–374
3. Weisberg, S. P., McCann, D., Desai, M., Rosenbaum, M., Leibel, R. L., and Ferrante, A. W., Jr. (2003) Obesity is associated with macrophage accumulation in adipose tissue. *J. Clin. Invest.* **112,** 1796–1808
4. Talukdar, S., Oh da, Y., Bandyopadhyay, G., Li, D., Xu, J., McNelis, J., Lu, M., Li, P., Yan, Q., Zhu, Y., Ofrecio, J., Lin, M., Brenner, M. B., and Olefsky, J. M. (2012) Neutrophils mediate insulin resistance in mice fed a high-fat diet through secreted elastase. *Nat. Med.* **18,** 1407–1412
5. Nishimura, S., Manabe, I., Nagasaki, M., Eto, K., Yamashita, H., Ohsugi, M., Otsu, M., Hara, K., Ueki, K., Sugiura, S., Yoshimura, K., Kadowaki, T., and Nagai, R. (2009) CD8+ effector T cells contribute to macrophage recruitment and adipose tissue inflammation in obesity. *Nat. Med.* **15,** 914–920
6. Wu, D., Molofsky, A. B., Liang, H. E., Ricardo-Gonzalez, R. R., Jouihan, H. A., Bando, J. K., Chawla, A., and Locksley, R. M. (2011) Eosinophils sustain adipose alternatively activated macrophages associated with glucose homeostasis. *Science* **332,** 243–247
7. Fujisaka, S., Usui, I., Bukhari, A., Ikutani, M., Oya, T., Kanatani, Y., Tsuneyama, K., Nagai, Y., Takatsu, K., Urakaze, M., Kobayashi, M., and Tobe, K. (2009) Regulatory mechanisms for adipose tissue M1 and M2 macrophages in diet-induced obese mice. *Diabetes* **58,** 2574–2582
8. de Alvaro, C., Teruel, T., Hernandez, R., and Lorenzo, M. (2004) Tumor necrosis factor α produces insulin resistance in skeletal muscle by activation of inhibitor κB kinase in a p38 MAPK-dependent manner. *J. Biol. Chem.* **279,** 17070–17078
9. Nguyen, M. T., Satoh, H., Favelyukis, S., Babendure, J. L., Imamura, T., Sbodio, J. I., Zalevsky, J., Dahiyat, B. I., Chi, N. W., and Olefsky, J. M. (2005) JNK and tumor necrosis factor-α mediate free fatty acid-induced insulin resistance in 3T3-L1 adipocytes. *J. Biol. Chem.* **280,** 35361–35371
10. Stienstra, R., Joosten, L. A., Koenen, T., van Tits, B., van Diepen, J. A., van den Berg, S. A., Rensen, P. C., Voshol, P. J., Fantuzzi, G., Hijmans, A., Kersten, S., Müller, M., van den Berg, W. B., van Rooijen, N., Wabitsch, M., Kullberg, B. J., van der Meer, J. W., Kanneganti, T., Tack, C. J., and Netea, M. G. (2010) The inflammasome-mediated caspase-1 activation controls adipocyte differentiation and insulin sensitivity. *Cell Metab.* **12,** 593–605
11. Jager, J., Grémeaux, T., Cormont, M., Le Marchand-Brustel, Y., and Tanti, J. F. (2007) Interleukin-1β-induced insulin resistance in adipocytes through down-regulation of insulin receptor substrate-1 expression. *Endocrinology* **148,** 241–251
12. Hong, E. G., Ko, H. J., Cho, Y. R., Kim, H. J., Ma, Z., Yu, T. Y., Friedline, R. H., Kurt-Jones, E., Finberg, R., Fischer, M. A., Granger, E. L., Norbury, C. C., Hauschka, S. D., Philbrick, W. M., Lee, C. G., Elias, J. A., and Kim, J. K. (2009) Interleukin-10 prevents diet-induced insulin resistance by attenuating macrophage and cytokine response in skeletal muscle. *Diabetes* **58,** 2525–2535
13. Gao, M., Zhang, C., Ma, Y., Bu, L., Yan, L., and Liu, D. (2013) Hydrodynamic delivery of mIL10 gene protects mice from high-fat diet-induced obesity and glucose intolerance. *Mol. Ther.* **21,** 1852–1861
14. Taga, T., and Kishimoto, T. (1997) Gp130 and the interleukin-6 family of cytokines. *Annu. Rev. Immunol.* **15,** 797–819
15. Tanaka, M., Hara, T., Copeland, N. G., Gilbert, D. J., Jenkins, N. A., and Miyajima, A. (1999) Reconstitution of the functional mouse oncostatin M (OSM) receptor: molecular cloning of the mouse OSM receptor β subunit. *Blood* **93,** 804–815
16. Tamura, S., Morikawa, Y., Miyajima, A., and Senba, E. (2002) Expression of oncostatin M in hematopoietic organs. *Dev. Dyn.* **225,** 327–331
17. Repovic, P., and Benveniste, E. N. (2002) Prostaglandin E2 is a novel inducer of oncostatin-M expression in macrophages and microglia. *J. Neurosci.* **22,** 5334–5343
18. Broxmeyer, H. E., Bruns, H. A., Zhang, S., Cooper, S., Hangoc, G., McKenzie, A. N., Dent, A. L., Schindler, U., Naeger, L. K., Hoey, T., and Kaplan, M. H. (2002) Th1 cells regulate hematopoietic progenitor cell homeostasis by production of oncostatin M. *Immunity* **16,** 815–825
19. Mozaffarian, A., Brewer, A. W., Trueblood, E. S., Luzina, I. G., Todd, N. W., Atamas, S. P., and Arnett, H. A. (2008) Mechanisms of oncostatin M-induced pulmonary inflammation and fibrosis. *J. Immunol.* **181,** 7243–7253
20. Wallace, P. M., MacMaster, J. F., Rouleau, K. A., Brown, T. J., Loy, J. K., Donaldson, K. L., and Wahl, A. F. (1999) Regulation of inflammatory responses by oncostatin M. *J. Immunol.* **162,** 5547–5555
21. Komori, T., Tanaka, M., Senba, E., Miyajima, A., and Morikawa, Y. (2013) Lack of oncostatin M receptor β leads to adipose tissue inflammation and insulin resistance by switching macrophage phenotype. *J. Biol. Chem.* **288,** 21861–21875
22. Tanaka, M., Hirabayashi, Y., Sekiguchi, T., Inoue, T., Katsuki, M., and Miyajima, A. (2003) Targeted disruption of oncostatin M receptor results in altered hematopoiesis. *Blood* **102,** 3154–3162
23. Racioppi, L., Noeldner, P. K., Lin, F., Arvai, S., Means, A. R. (2012) Calcium/calmodulin-dependent protein kinase kinase 2 regulates macrophage-mediated inflammatory responses. *J. Biol. Chem.* **287,** 11579–11591
24. Komori, T., Doi, A., Nosaka, T., Furuta, H., Akamizu, T., Kitamura, T., Senba, E., and Morikawa, Y. (2012) Regulation of AMP-activated protein kinase signaling by AFF4 protein, member of AF4 (ALL1-fused gene from chromosome 4) family of transcription factors, in hypothalamic neurons. *J. Biol. Chem.* **287,** 19985–19996
25. Komori, T., Doi, A., Furuta, H., Wakao, H., Nakao, N., Nakazato, M., Nanjo, K., Senba, E., and Morikawa, Y. (2010) Regulation of ghrelin signaling by a leptin-induced gene, negative regulatory element-binding protein, in the hypothalamic neurons. *J. Biol. Chem.* **285,** 37884–37894
26. Folch, J., Lees, M., and Sloane Stanley, G. H. (1957) A simple method for the isolation and purification of total lipides from animal tissues. *J. Biol. Chem.* **226,** 497–509
27. Owen, J. L., Zhang, Y., Bae, S. H., Farooqi, M. S., Liang, G., Hammer, R. E., Goldstein, J. L., and Brown, M. S. (2012) Insulin stimulation of SREBP-1c processing in transgenic rat hepatocytes requires p70 S6-kinase. *Proc. Natl. Acad. Sci. U.S.A.* **109,** 16184–16189
28. Puigserver, P., Rhee, J., Donovan, J., Walkey, C. J., Yoon, J. C., Oriente, F., Kitamura, Y., Altomonte, J., Dong, H., Accili, D., Spiegelman, B. M. (2003) Insulin-regulated hepatic gluconeogenesis through FOXO1-PGC-1α interaction. *Nature* **423,** 550–555
29. Bae, E. J., Xu, J., Oh, D. Y., Bandyopadhyay, G., Lagakos, W. S., Keshwani,

M., Olefsky, J. M. (2012) Liver-specific p70 S6 kinase depletion protects against hepatic steatosis and systemic insulin resistance. *J. Biol. Chem.* **287,** 18769–18780
30. Kamiya, A., Kinoshita, T., Ito, Y., Matsui, T., Morikawa, Y., Senba, E., Nakashima, K., Taga, T., Yoshida, K., Kishimoto, T., and Miyajima, A. (1999) Fetal liver development requires a paracrine action of oncostatin M through the gp130 signal transducer. *EMBO J.* **18,** 2127–2136
31. Morikawa, Y., Tamura, S., Minehata, K., Donovan, P. J., Miyajima, A., and Senba, E. (2004) Essential function of oncostatin m in nociceptive neurons of dorsal root ganglia. *J. Neurosci.* **24,** 1941–1947
32. Mukouyama, Y., Hara, T., Xu, M., Tamura, K., Donovan, P. J., Kim, H., Kogo, H., Tsuji, K., Nakahata, T., and Miyajima, A. (1998) *In vitro* expansion of murine multipotential hematopoietic progenitors from the embryonic aorta-gonad-mesonephros region. *Immunity* **8,** 105–114
33. Wallenius, V., Wallenius, K., Ahrén, B., Rudling, M., Carlsten, H., Dickson, S. L., Ohlsson, C., and Jansson, J. O. (2002) Interleukin-6-deficient mice develop mature-onset obesity. *Nat. Med.* **8,** 75–79
34. Watt, M. J., Dzamko, N., Thomas, W. G., Rose-John, S., Ernst, M., Carling, D., Kemp, B. E., Febbraio, M. A., and Steinberg, G. R. (2006) CNTF reverses obesity-induced insulin resistance by activating skeletal muscle AMPK. *Nat. Med.* **12,** 541–548
35. Moreno-Aliaga, M. J., Pérez-Echarri, N., Marcos-Gómez, B., Larequi, E., Gil-Bea, F. J., Viollet, B., Gimenez, I., Martínez, J. A., Prieto, J., and Bustos, M. (2011) Cardiotrophin-1 is a key regulator of glucose and lipid metabolism. *Cell Metab.* **14,** 242–253
36. Mehran, A. E., Templeman, N. M., Brigidi, G. S., Lim, G. E., Chu, K. Y., Hu, X., Botezelli, J. D., Asadi, A., Hoffman, B. G., Kieffer, T. J., Bamji, S. X., Clee, S. M., Johnson, J. D. (2012) Hyperinsulinemia drives diet-induced obesity independently of brain insulin production. *Cell Metab.* **16,** 723–737
37. O'Rourke, R. W., White, A. E., Metcalf, M. D., Winters, B. R., Diggs, B. S., Zhu, X., and Marks, D. L. (2012) Systemic inflammation and insulin sensitivity in obese IFN-γ knockout mice. *Metabolism* **61,** 1152–1161
38. Grzelkowska-Kowalczyk, K., and Wieteska-Skrzeczyńska, W. (2010) Treatment with IFN-γ prevents insulin-dependent PKB, p70S6k phosphorylation and protein synthesis in mouse C2C12 myogenic cells. *Cell Biol. Int.* **34,** 117–124
39. Feuerer, M., Herrero, L., Cipolletta, D., Naaz, A., Wong, J., Nayer, A., Lee, J., Goldfine, A. B., Benoist, C., Shoelson, S., Mathis, D. (2009) Lean, but not obese, fat is enriched for a unique population of regulatory T cells that affect metabolic parameters. *Nat. Med.* **15,** 930–939
40. Goerdt, S., and Orfanos, C. E. (1999) Other functions, other genes: alternative activation of antigen-presenting cells. *Immunity* **10,** 137–142
41. Tilg, H., and Moschen, A. R. (2008) Insulin resistance, inflammation, and non-alcoholic fatty liver disease. *Trends Endocrinol. Metab.* **19,** 371–379
42. Michelotti, G. A., Machado, M. V., and Diehl, A. M. (2013) NAFLD, NASH, and liver cancer. *Nat. Rev. Gastroenterol. Hepatol.* **10,** 656–665
43. Li, S., Brown, M. S., and Goldstein, J. L. (2010) Bifurcation of insulin signaling pathway in rat liver: mTORC1 required for stimulation of lipogenesis, but not inhibition of gluconeogenesis. *Proc. Natl. Acad. Sci. U.S.A.* **107,** 3441–3446
44. Sun, Z., and Lazar, M. A. (2013) Dissociating fatty liver and diabetes. *Trends Endocrinol. Metab.* **24,** 4–12
45. Michael, M. D., Kulkarni, R. N., Postic, C., Previs, S. F., Shulman, G. I., Magnuson, M. A., and Kahn, C. R. (2000) Loss of insulin signaling in hepatocytes leads to severe insulin resistance and progressive hepatic dysfunction. *Mol. Cell* **6,** 87–97
46. Biddinger, S. B., Hernandez-Ono, A., Rask-Madsen, C., Haas, J. T., Alemán, J. O., Suzuki, R., Scapa, E. F., Agarwal, C., Carey, M. C., Stephanopoulos, G., Cohen, D. E., King, G. L., Ginsberg, H. N., and Kahn, C. R. (2008) Hepatic insulin resistance is sufficient to produce dyslipidemia and susceptibility to atherosclerosis. *Cell Metab.* **7,** 125–134
47. Stiles, B., Wang, Y., Stahl, A., Bassilian, S., Lee, W. P., Kim, Y. J., Sherwin, R., Devaskar, S., Lesche, R., Magnuson, M. A., and Wu, H. (2004) Liver-specific deletion of negative regulator Pten results in fatty liver and insulin hypersensitivity. *Proc. Natl. Acad. Sci. U.S.A.* **101,** 2082–2087
48. Brown, M. S., and Goldstein, J. L. (2008) Selective versus total insulin resistance: a pathogenic paradox. *Cell Metab.* **7,** 95–96
49. Benhamed, F., Denechaud, P. D., Lemoine, M., Robichon, C., Moldes, M., Bertrand-Michel, J., Ratziu, V., Serfaty, L., Housset, C., Capeau, J., Girard, J., Guillou, H., and Postic, C. (2012) The lipogenic transcription factor ChREBP dissociates hepatic steatosis from insulin resistance in mice and humans. *J. Clin. Invest.* **122,** 2176–2194
50. Beaven, S. W., Matveyenko, A., Wroblewski, K., Chao, L., Wilpitz, D., Hsu, T. W., Lentz, J., Drew, B., Hevener, A. L., and Tontonoz, P. (2013) Reciprocal regulation of hepatic and adipose lipogenesis by liver x receptors in obesity and insulin resistance. *Cell Metab.* **18,** 106–117
51. Zhou, Y., Abidi, P., Kim, A., Chen, W., Huang, T. T., Kraemer, F. B., Liu, J. (2007) Transcriptional activation of hepatic ACSL3 and ACSL5 by oncostatin M reduces hypertriglyceridemia through enhanced β-oxidation. *Arterioscler. Thromb. Vasc. Biol.* **27,** 2198–2205

The American Journal of Pathology, Vol. 184, No. 8, August 2014

ELSEVIER

The American Journal of
PATHOLOGY

ajp.amjpathol.org

GASTROINTESTINAL, HEPATOBILIARY, AND PANCREATIC PATHOLOGY

Semaphorin 3E Secreted by Damaged Hepatocytes Regulates the Sinusoidal Regeneration and Liver Fibrosis during Liver Regeneration

Tomoki Yagai,* Atsushi Miyajima,* and Minoru Tanaka[†‡]

From the Laboratories of Cell Growth and Differentiation and Stem Cell Regulation,[†] Institute of Molecular and Cellular Biosciences, The University of Tokyo, Tokyo; and the Department of Regenerative Medicine,[‡] Research Institute, National Center for Global Health and Medicine, Tokyo, Japan*

Accepted for publication
April 28, 2014.

Address correspondence to Minoru Tanaka, Ph.D., Laboratory of Stem Cell Regulation, Institute of Molecular and Cellular Biosciences, The University of Tokyo, 1-1-1 Yayoi, Bunkyo-ku, Tokyo 113-0032, Japan. E-mail: tanaka@iam.u-tokyo.ac.jp.

The liver has a remarkable capacity to regenerate after injury. Although the regulatory mechanisms of hepatocytic regeneration have been a subject of intense study, the dynamism of the sinusoids, specialized blood vessels in the liver, remains largely unknown. Transient activation of hepatic stellate cells and hepatic sinusoidal endothelial cells, which constitute the sinusoids, contributes to liver regeneration during acute injury, whereas their sustained activation causes liver fibrosis during chronic injury. We focused on understanding the association between damaged hepatocytes and sinusoidal regeneration or liver fibrogenesis using a carbon tetrachloride–induced liver injury mouse model. Damaged hepatocytes rapidly expressed semaphorin 3E (Sema3e), which induced contraction of sinusoidal endothelial cells and thereby contributed to activating hepatic stellate cells for wound healing. In addition, ectopic and consecutive expression of Sema3e in hepatocytes by the hydrodynamic tail-vein injection method resulted in disorganized regeneration of sinusoids and sustained activation of hepatic stellate cells. In contrast, liver fibrosis ameliorated in *Sema3e*-knockout mice compared with wild-type mice in a chronic liver injury model. Our results indicate that Sema3e, secreted by damaged hepatocytes, affects sinusoidal regeneration in a paracrine manner during liver regeneration, suggesting that Sema3e is a novel therapeutic target in liver fibrogenesis. *(Am J Pathol 2014, 184: 2250–2259; http://dx.doi.org/10.1016/j.ajpath.2014.04.018)*

The liver has a remarkable capacity to regenerate from surgical resection and damage caused by various insults, such as toxic chemicals and viral infection. Many injuries cause death of hepatocytes, which are liver parenchymal cells, followed by compensatory proliferation of the remaining hepatocytes to regenerate.[1] Therefore, the mechanisms of liver regeneration are focused on hepatocytes,[2,3] whereas the regenerative process of sinusoids, unique capillary vessels in the liver, remains largely unknown. The hepatic sinusoid is composed of fenestrated sinusoidal endothelial cells (SECs) and hepatic stellate cells (HSCs). In general, the process of liver regeneration after injury is accompanied by sinusoid fibrogenesis. Although transient fibrogenesis is beneficial for wound healing by providing mechanical stability and a scaffold for hepatocytic regeneration,[4] prolonged fibrogenesis during chronic hepatitis often leads to the accumulation of extracellular matrix (ECM), resulting in nodule formation and alterations in hepatic function and blood flow. Therefore, liver fibrosis is a pathologic sign that results in severe hepatic diseases, such as cirrhosis and carcinogenesis.[5] Previous studies have revealed that HSCs, characteristic pericytes that line the hepatic sinusoid, are a key cellular source for the ECM and that activated HSCs acquire myofibroblastic characteristics by secreting excess ECM protein, such as collagen types I and III.[6] In addition, SECs and HSCs cooperate to maintain the sinusoidal environment. For example, vascular endothelial growth factor (VEGF) secreted by HSCs maintains SEC homeostasis by preventing their capillarization.[7] Conversely, SECs revert activated HSCs to a

Supported in part by Grants-in-Aid for Scientific Research 22590719 and 22118006 from the Japan Society for the Promotion of Science, Japan (A.M. and M.T.).

Disclosures: None declared.

http://dx.doi.org/10.1016/j.ajpath.2014.04.018

quiescent status via nitric oxide synthesis.[8] These observations suggest that the reciprocal cell-to-cell communication between SECs and HSCs is critical for sinusoidal regeneration and liver fibrosis after liver injury and that SEC angiogenic factors could be the regulators of liver fibrogenesis through indirect activation of HSCs. Because liver injury is accompanied by inflammation and hepatocytic insults, inflammatory cells are involved in sinusoidal fibrogenesis.[9] In addition, molecules secreted from damaged hepatocytes contribute to the compensatory proliferation of surrounding hepatocytes.[10,11] However, whether there is a direct association between damaged hepatocytes and sinusoidal regeneration or liver fibrogenesis is currently unknown.

We found that semaphorin 3E (Sema3e) is up-regulated by 3,5-diethoxycarbonyl-1,4-dihydrocollidine feeding in a mouse model of chronic hepatitis.[12,13] Sema3e is a secretory protein that belongs to the class 3 semaphorin family[14] and plays a neurogenic and angiogenic repulsive role in development.[15,16] The receptors for semaphorins are plexins and neuropilins, and Sema3e specifically binds to plexin D1 (Plxnd1).[17] Sakurai et al[18] reported that Sema3e/Plxnd1 signaling initiates the antiangiogenic response by regulating Arf6 and R-Ras, inhibiting endothelial tip cell adhesion to the ECM, and retracting filopodia. Moreover, the Sema3e/Plxnd1 axis interferes with VEGF and VEGF receptor (VEGFR)-2 signaling via a feedback mechanism.[19] Indeed, Sema3e/Plxnd1 signaling plays an essential role in development because *Sema3e*-knockout (KO) mice display aberrant vascularization of intersomitic blood vessels.[17] However, the involvement of Sema3e/Plxnd1 signaling in liver regeneration and pathogenesis remains largely unknown. In this study, we focused on the mechanisms of sinusoidal regeneration after liver injury and found that Sema3e produced by damaged hepatocytes activates SECs via Plxnd1 and thereby plays a critical role in sinusoidal regeneration and liver fibrosis.

Materials and Methods

Mice

C57BL/6 mice were obtained from CLEA Japan (Tokyo, Japan). *Sema3e*-KO mice were provided by Dr. Yutaka Yoshida (Cincinnati Children's Hospital Medical Center, Cincinnati, OH).[17] The littermates were subjected to carbon tetrachloride (CCl_4)—induced liver fibrosis. All animal experiments were performed in accordance with our institutional guidelines.

Induction of CCl_4-Induced Acute Liver Injury and Liver Fibrosis

Acute liver injury was induced by single i.p. injection of CCl_4. CCl_4 (Wako Pure Chemical, Osaka, Japan) was diluted in corn oil (Wako) to 20% and injected into mice at a dose of 1 mL/kg of CCl_4. Liver fibrosis was induced by repeated injection of CCl_4, twice per week for 4 weeks. Livers were harvested 3 days after the final CCl_4 injection.

H&E and Sirius Red Staining

Liver cryosections (8 μm) were mounted on glass slides and fixed with Zamboni fixative solution for 10 minutes for immunostaining. The fixed sections were incubated with 5% skim milk (w/v) in phosphate-buffered saline and then incubated with primary antibodies, followed by secondary antibodies. The antibodies used in this study are listed in Table 1. Images were captured using Observer Z1 with an AxioCam HRc (Zeiss, Oberkochen, Germany). The hematoxylin and eosin (H&E) staining was performed after immunostaining in some specific experiments as stated later. The cover glass on enclosed sections was eliminated carefully with adequate phosphate-buffered saline (Wako) and then stained with H&E (Muto Pure Chemicals, Tokyo, Japan). Sirius Red staining was performed followed by Bouin's solution (Sigma-Aldrich, St. Louis, MO) fixation, as described previously. In brief, nuclei were stained with Weigert's iron hematoxylin (Wako) and then stained with collagen and Direct Red 80 (Sigma-Aldrich).

RT-PCR and Real-time RT-PCR

Total RNA was isolated from mouse livers or hepatic cells using TRIzol reagent (Invitrogen). Reverse transcription to cDNA templates was performed using random primers and a High-Capacity cDNA Reverse-Transcription Kit (Applied Biosystems, Foster City, CA). Real-time RT-PCR experiments were conducted with a LightCycler 480 system and Universal Probe Library (Roche Diagnostics, Indianapolis, IN). The mouse *ACTB* gene assay in ProbeLibrary was used as the normalization control. The sequence information for the primer pairs used is listed in Table 2. Probes #63 and #27 were used for *Sema3e* and *Plxnd1*, respectively. Sema3e primers were used for experiments by analyzing the Sema3e expression. Sema3e vector primers were used to construct the expression vector.

Table 1 Antibodies Used in the Study

Protein	Supplier
Semaphorin 3E (Sema3e)	Abgent (San Diego, CA)
Stabilin-2 (Stab-2)	Nonaka et al[20]
CD45	BD Biosciences (San Diego, CA)
Nerve growth factor receptor (NGFR, p75NTR)	R&D Systems (Minneapolis, MN)
Actin, α_2, smooth muscle, aorta (α-SMA)	Abcam (Cambridge, MA)
CD16/CD32 (FcγIII/II Receptor)	BD Biosciences
Ki-67	eBioscience (San Diego, CA)
Collagen I	AbD Serotec (Kidlington, UK)
Phalloidin	Invitrogen (Carlsbad, CA)
GAPDH	Merck Millipore (Billerica, MA)

α-SMA, α-smooth muscle actin; GAPDH, glyceraldehyde-3-phosphate dehydrogenase; p75NTR, p75 low-affinity neurotrophic growth factor receptor.

Table 2 Primer Sequences Used for This Study

Gene	Sense primer sequence	Antisense primer sequence
Sema3e	5′-GGGGCAGATGTCCTTTTGA-3′	5′-AGTCCAGCAAACAGCTCATTC-3′
Plxnd1	5′-CTGGATGTCCATCTGCATGT-3′	5′-CAGGAAGAACGGCTCACCTA-3′
Construction for *Sema3e* expression vector	5′-AGCTAGCCCCTGGAGGGAAGTACTAA-3′	5′-GTCGACTCCTAGGTTCCTCAGCCGCC-3′

Cell Isolation

A single-cell suspension was obtained from the liver by a modified collagenase perfusion method, as described previously.[21] In brief, liver specimens were perfused with a basic perfusion solution containing 0.5 g/L of collagenase-Yakult (Yakult Pharmaceutical Industry Co. Ltd., Tokyo, Japan) and 50 mg/L of DNase I (Sigma-Aldrich). The digested liver was passed through a 70-μm cell strainer. After centrifugation at 60 × *g* for 1 minute, the precipitated cells were used as hepatocytes after Percoll (GE Healthcare, Piscataway, NJ) density centrifugation. The supernatant was transferred to a new tube and centrifuged at 120 × *g* for 2 minutes repeatedly until no pellet was visible. The final supernatant was centrifuged at 340 × *g* for 5 minutes, and the precipitated cells were used as non-parenchymal cells for cell isolation. Aliquots of cells were blocked with anti-FcγR antibody, co-stained with fluorescence- and/or biotin-conjugated antibodies, and then incubated with allophycocyanin-conjugated streptavidin (BD Biosciences, San Diego, CA) if needed. The samples were sorted by Moflo XDP (Beckman-Coulter, Fullerton, CA) or auto-MACS pro (Miltenyi Biotec, Bergisch Gladbach, Germany) with anti-allophycocyanin microbeads. Dead cells were excluded by propidium iodide staining.

Primary Culture of Hepatocytes and SECs

Primary hepatocytes separated by Percoll were seeded in type I collagen–coated 6-well dishes (BD Biosciences) at 5 × 10^5 per well with William's Medium E (Life Technologies, Carlsbad, CA) that contained 10% fetal bovine serum (JRH Biosciences, Lenexa, KS). After 3 hours (0 hours), unattached hepatocytes were washed out, and dimethyl sulfoxide (vehicle) or CCl_4 dissolved in dimethyl sulfoxide was added to the culture medium at a final concentration of 2.0 mmol/L. Then, total RNA was extracted from hepatocytes at 0, 3, 6, and 24 hours after CCl_4 administration. Isolated primary SECs were seeded in dishes coated with collagen type I-C (Nitta gelatin, Osaka, Japan) with Dulbecco's modified Eagle's medium/Ham's nutrient mixture F-12 (Sigma-Aldrich). After 12 hours, recombinant mouse Sema3e (R&D Systems) was added to the culture medium for a final concentration of 500 ng/mL. After incubation for 30 minutes, the morphologic status of SECs was analyzed by immunocytochemistry using fluorescein-conjugated phalloidin and Hoechst stain.

Forced Expression of Sema3e in Hepatocytes

We used the pLIVE vector and TransIT-EE Hydrodynamic Delivery solution (Mirus Bio, Madison, WI) to introduce Sema3e cDNA into 8-week-old mice by hydrodynamic tail-vein injection (HTVi). The primer pairs used for the expression vector are listed in Table 2.

Quantitative Analysis of Liver Sections Stained with Immunohistochemistry and Sirius Red

The vascular density was determined by analyzing stabilin (Stab)-2–positive area in the fields, including the central vein (CV). Four independent images of liver sections at ×200 magnification per animal were analyzed using the ImageJ software version 1.46r (NIH, Bethesda, MD). The parenchymal area was evaluated by subtracting vascular luminal area from the total field area and used for calculation. The fibrosis area was assessed by analyzing the Sirius Red–stained collagen areas in the liver sections at ×50 magnification. Ki-67–positive hepatocytes were counted using In Cell Analyzer 2000 (GE Healthcare), as described previously.[22]

Measurement of Serum ALT, Serum Albumin, and Hydroxyproline Content

Serum alanine aminotransferase (ALT) and albumin were measured at the Oriental Yeast Company (Tokyo, Japan) or by the Transaminase CII-test Wako (Wako). Hydroxyproline content was measured as described previously.[23]

Statistical Analysis

Statistical analysis was performed using the unpaired two-tailed Student's *t*-test. Gene expression in multiple liver cell fractions was compared by one-way analysis of variance and subsequent Tukey's tests. $P < 0.05$ was considered statistically significant.

Results

Sinusoidal Regeneration in CCl_4-Induced Liver Injury in Mice

The i.p. injection of CCl_4 produces a conventional liver injury model to study liver regeneration and subsequent fibrosis. We treated mice with CCl_4 and monitored the status of hepatocytes and SECs to investigate sinusoidal regeneration after liver injury. We have reported previously that Stab-2, a scavenger receptor, and receptors II (CD32) and III (CD16) for Fc fragment of IgG (FcγRs) are highly expressed in SECs and make it possible to distinguish SECs from other kinds of endothelial cells.[20,24] Frozen liver sections were subjected to immunohistochemistry (IHC) using

anti–Stab-2 or anti-FcγR antibodies, followed by H&E staining to visualize SECs in CCl_4-treated liver. Sinusoids in normal liver (0 hours) extended from the CV in a high-density radial pattern (Figure 1, A and B, and Supplemental Figure S1, A and B). Because CCl_4 is metabolized by cytochrome P450 in hepatocytes surrounding the CV to produce toxic free radicals as intermediate metabolites,[25] administering CCl_4 causes massive hepatocytic death around the CV. H&E staining revealed mild and obvious degeneration of hepatocytes at 24 and 48 hours after CCl_4 treatment, respectively (Figure 1, C and E, and Supplemental Figure S1, C and E). The sinusoidal structure was disorganized 24 hours after CCl_4 treatment, and most SECs in the degenerated region (Figure 1) seemed to be contracted, suggesting that some substantial alterations occurred in the SECs (Figure 1, C and D, and Supplemental Figure S1, C and D). The degenerated region became more obvious, and the arrangement of SECs remained disorganized 48 hours after CCl_4 treatment (Figure 1, E and F, and Supplemental Figure S1, E and F). Degeneration of hepatocytes decreased and hepatocytes regenerated 72 and 96 hours after CCl_4 treatment, but immune cells accumulated around the CV (Figure 1, G and I, and Supplemental Figure S1, G and I). In contrast, SECs returned to their original position and morphologic status during these phases (Figure 1, H and J, and Supplemental Figure S1, H and J). These data suggest that the process of sinusoidal regeneration would be completed by 72 hours after CCl_4-induced injury in mice.

Sema3e Is Expressed by Degenerating Hepatocytes during CCl_4-Induced Liver Injury

Because a sign of contraction was observed in SECs at 24 hours after CCl_4 treatment, it was supposed that some angiogenesis-related factors might be involved in this morphologic change. We found in our previous research about liver regeneration during chronic hepatitis that Sema3e is up-regulated in injured liver. Therefore, we examined the Sema3e expression pattern by quantitative RT-PCR (RT-qPCR) after CCl_4 treatment and measured serum concentrations of ALT as a liver injury marker (Figure 2, A and B). As a result, Sema3e expression was negligible in normal liver but was up-regulated drastically at 24 hours after CCl_4 treatment. Intriguingly, Sema3e expression then decreased sharply at 48 hours and returned to the basal level after 72 hours. These results suggest that up-regulation of Sema3e might be related with degeneration of hepatocytes, as evaluated by serum ALT (Figure 2, A and B), whereas rapid Sema3e down-regulation may represent completion of hepatocytic death. Therefore, we hypothesized that damaged hepatocytes could be a source for Sema3e. To address this hypothesis, we examined Sema3e expression in injured liver sections by IHC using an anti-Sema3e antibody. As expected, strong Sema3e signals were detected within the degenerating area around the CV 24 hours after CCl_4 treatment (Figure 2C). To investigate whether the cells expressing Sema3e were hepatocytes, we stimulated hepatocytes isolated from normal liver with CCl_4 in culture. Primary cultured hepatocytes became

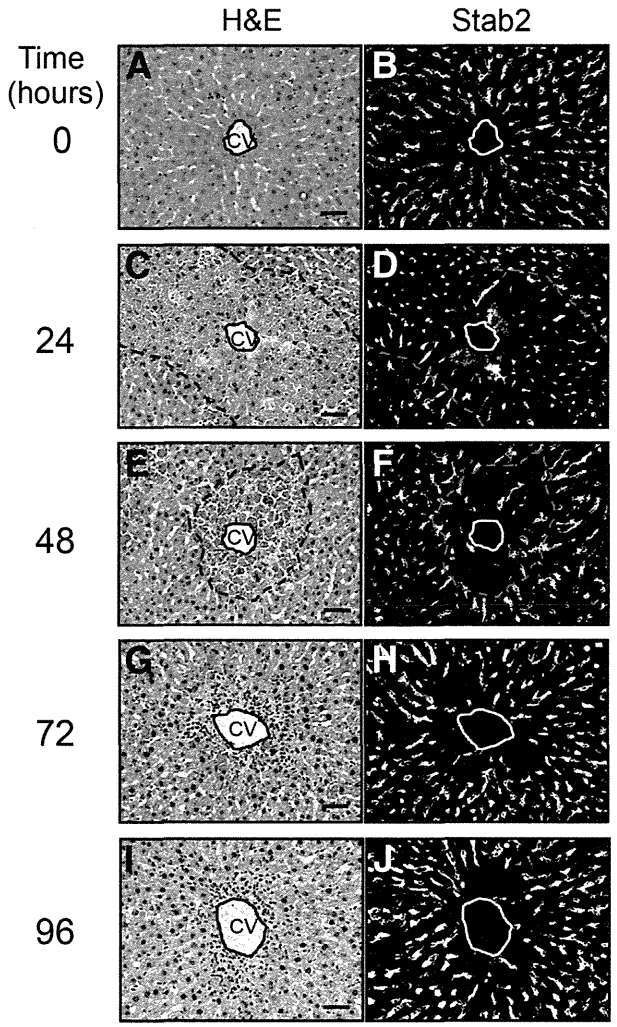

Figure 1 Morphologic transition of sinusoids after carbon tetrachloride (CCl_4)–induced liver injury. Identical sections were subjected to immunohistochemistry using anti-stabilin (Stab)-2 antibody and hematoxylin and eosin (H&E) staining (after immunostaining). **A** and **B**: The sinusoids extend from the central vein (CV) in a high-density radial pattern in normal liver (0 hours) before injury. **C** and **D:** Sinusoidal structure is affected 24 hours after CCl_4 treatment, followed by hepatocyte degeneration around the CV. **E** and **F:** Most sinusoidal endothelial cells (SECs) in the degenerated region (surrounded by the broken line) are strongly contracted. The arrangement of SECs remains disordered 48 hours after CCl_4 treatment. Degeneration of hepatocytes diminishes 72 (**G** and **H**) and 96 hours (**I** and **J**) after CCl_4 treatment, hepatocytes regenerate, and immune cells accumulate around the CV. Most of the SECs were stationed at the proper position during these phases. Scale bars: 50 μm (**A**, **C**, **E**, **G**, and **I**).

gradually swollen after CCl_4 treatment, and most of the hepatocytes degenerated 24 hours after CCl_4 challenge (Figure 2D). Real-time RT-PCR revealed that the expression level of Sema3e of CCl_4-treated hepatocytes was significantly increased compared with that of vehicle-treated or nontreated hepatocytes and 3.7-fold higher than that of injured liver 24 hours after *in vivo* administration of CCl_4 (whole liver), suggesting that damaged hepatocyte by oxidative stress is a major source of robust expression of Sema3e in CCl_4 injury model (Figure 2E). Although Sema3e is expressed in immune cells,[26] $CD45^+$ blood cells isolated from CCl_4-treated liver hardly expressed

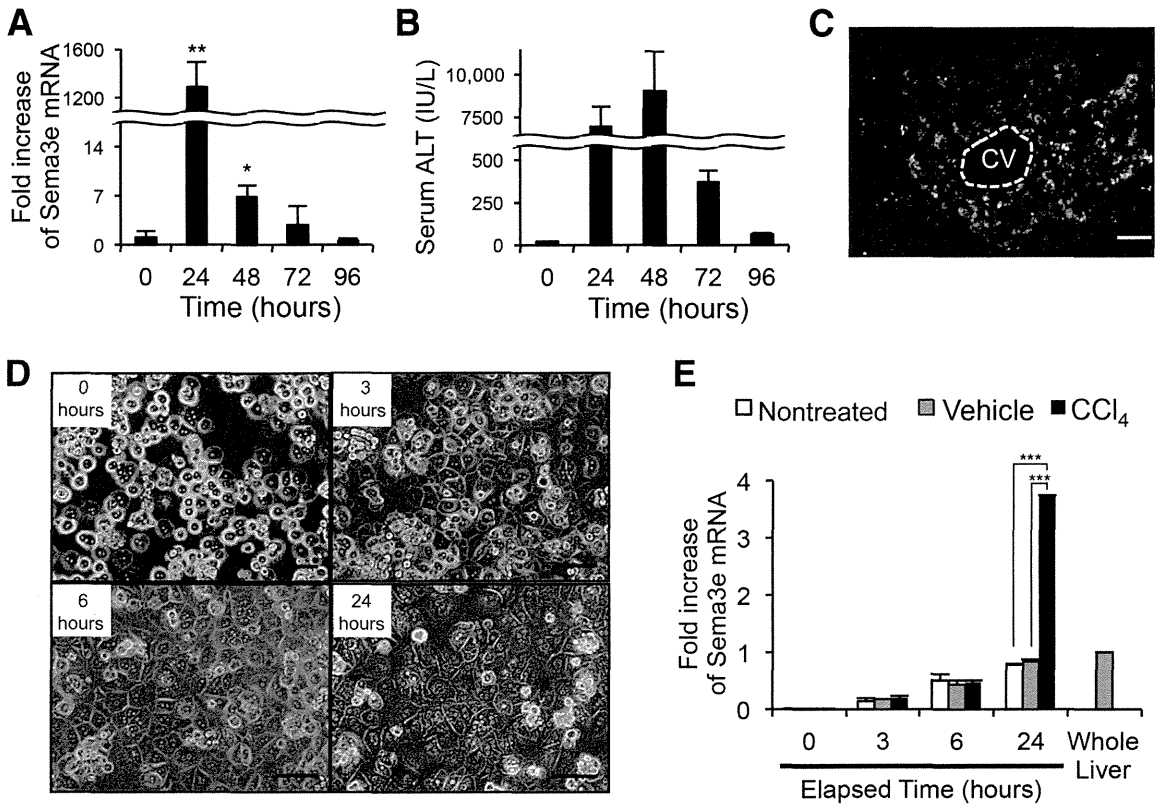

Figure 2 Expression profiles of semaphorin 3E (Sema3e) and plexin D1 (Plxnd1) in liver. **A:** Sema3e expression level in liver after carbon tetrachloride (CCl_4)—induced injury. **B:** Whole liver total RNA was assessed by quantitative RT-PCR. Evaluation of serum alanine aminotransferase level at indicated time points. **C:** Livers were subjected to immunohistochemical staining with an anti-Sema3e antibody 24 hours after CCl_4 treatment. Sema3e expression is observed in hepatocytes in the damaged region around the central vein. **D:** Morphologic alterations in primary cultured hepatocytes treated with CCl_4. **E:** The expression levels for *Sema3e* of primary cultured hepatocytes at 0, 3, 6, and 24 hours after nontreatment, vehicle treatment, or CCl_4 treatment, respectively. The whole liver represents the mRNA of injured mouse liver 24 hours after CCl_4 administration. The fold expression of Sema3e mRNA of cultured hepatocytes relative to the whole liver is shown. Data are expressed as means ± SEM. $n = 3$ per group. $^*P < 0.05$, $^{**}P < 0.01$, and $^{***}P < 0.001$ versus 0 hours after CCl_4 treatment. Scale bars: 50 μm (**C**); 100 μm (**D**).

Sema3e (Supplemental Figure S2A). Moreover, Sema3e was not induced after a 70% partial hepatectomy, which was not accompanied by hepatocyte damage (Supplemental Figure S2B). These results strongly suggest that Sema3e is induced in hepatocytes *in vitro* and *in vivo* in a damage-dependent manner.

Sema3e Has an Effect on Retracting SEC Filopodia

We isolated each type of liver cell by fluorescence-activated cell sorting and analyzed Sema3e receptor (Plxnd1) expression by RT-qPCR to identify the cell type that responded to Sema3e in injured liver. Plxnd1 was predominantly expressed in Stab-2^+ SECs (Figure 3A), suggesting that Sema3e secreted from degenerating hepatocytes could affect SECs in a paracrine fashion. Sema3e plays a role in repulsing the endothelial tip and inhibiting cell migration. However, the effect of Sema3e on SECs has not been examined. Therefore, we investigated the effect of Sema3e on freshly isolated SECs in culture. As a result, SEC filopodia retracted significantly in the presence of Sema3e (Figure 3, B and C), as reported previously in other endothelial cell lines.[18,27]

Prolonged Expression of Sema3e Results in Disoriented Sinusoidal Regeneration

Given that Sema3e also induced retraction of SEC filopodia *in vivo*, transient expression of Sema3e from damaged hepatocytes could be involved in the morphologic contraction of SECs as observed 24 hours after CCl_4 treatment (Figure 1D and Supplemental Figure S1D). This idea was supported by the result that SECs returned to their original morphologic status during reconstruction of sinusoids after the drastic decrease in Sema3e expression. To further verify Sema3e function *in vivo*, we examined the effect of prolonged Sema3e expression by HTVi, which is a method of delivering an expression vector into hepatocytes. We initially injected either Sema3e or a control expression vector into wild-type mice by HTVi. Then, each mouse was treated with either CCl_4 or vehicle 3 days after HTVi. We first examined SEC by using H&E and IHC staining 1 day after CCl_4 administration when endogenous Sema3e expression is drastically induced. We observed no obvious differences in the damaged area between control- and Sema3e-HTVi liver (Supplemental Figure S3). These results

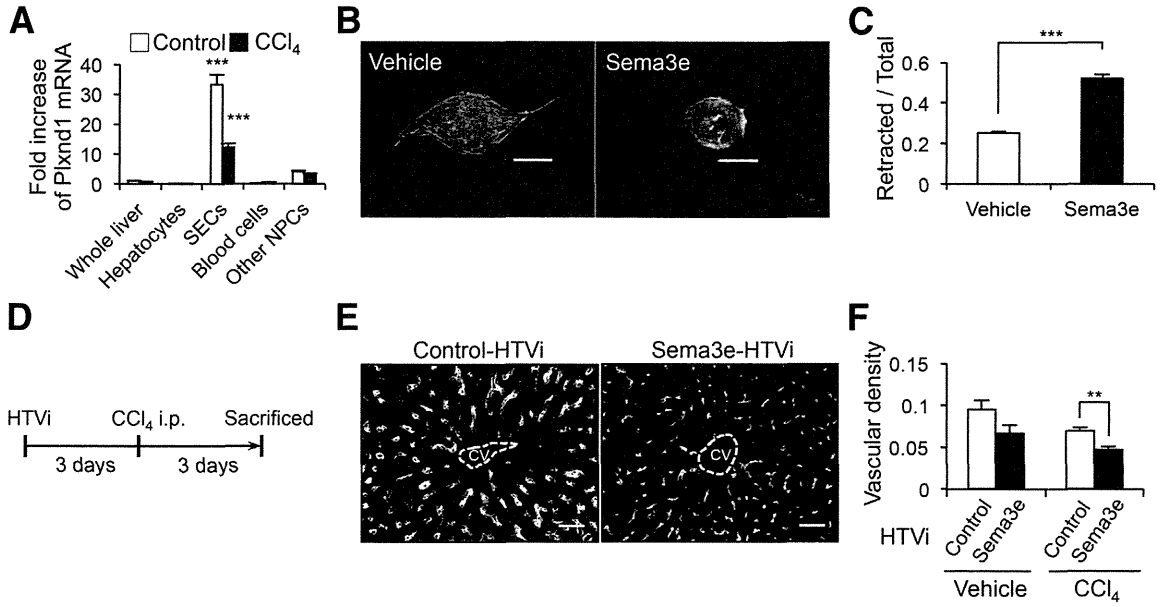

Figure 3 Semaphorin 3E (Sema3e) induces contraction of sinusoidal endothelial cells (SECs). **A:** Real-time RT-PCR analysis of plexin D1 (Plxnd1) in hepatocytes, SECs, blood cells, and other non-parenchymal cells (NPCs). Each fraction was isolated from normal or 24-hour post—carbon tetrachloride (CCl_4) liver, and Plxnd1 mRNA levels were compared with those of whole livers. Remarkable Plxnd1 expression was observed in SECs in normal and 24-hour post-CCl_4 livers. **B:** Morphologic changes in SECs after addition of Sema3e. **C:** SECs were subjected to primary culture with or without Sema3e. SECs cultured with Sema3e have significant retraction of filopodia observed in control SECs. **D:** Scheme of *in vivo* analysis using the hydrodynamic tail-vein injection (HTVi) method. **E:** The Sema3e expression vector was introduced into hepatocytes using the HTVi method. The mice were subjected to CCl_4 injection after 3 days. Then, livers were harvested after an additional 3 days. Immunostaining of liver sections with an anti—stabilin (Stab)-2 antibody 3 days after injury. **F:** Normal sinusoidal regeneration is observed in the control liver, whereas disorganized regeneration of contracted SECs is observed in Sema3e-expressed livers. Vascular density of control- and Sema3e-expressed liver sections before and after injury. The SEC area significantly decreases in Sema3e-expressed livers after liver injury. Vascular area was measured as Stab-2—positive area visualized by immunohistochemistry. Empty areas, such as the lumen, were subtracted for calculation. Data are expressed as means ± SEM. $n = 3$ per group (**A**); $n = 4$ per group (**C**); $n = 4$ to 5 per group (**F**). $^{**}P < 0.01$, $^{***}P < 0.001$ for analysis of variance with Tukey's post hoc tests. Scale bars: 20 μm (**D**); 50 μm (**F**).

suggested that the additional overexpression of Sema3e was not effective because the amount of endogenous Sema3e was enough to affect sinusoidal contraction 1 day after liver injury. Then, we analyzed the livers 3 days after CCl_4 administration when endogenous Sema3e expression is decreased (Figure 3D). Sinusoidal regeneration and SEC status were evaluated by IHC using an anti—Stab-2 antibody and vascular density, as represented by the ratio of the Stab-2—positive area to total parenchymal area (Figure 3, E and F). We confirmed that exogenous Sema3e expression by HTVi was maintained irrespective of CCl_4 treatment (Supplemental Figure S4). Although the vascular system of Sema3e-HTVi livers tended to decrease compared with that of control-HTVi livers, no significant difference was observed in vehicle treatment (Figure 3F). The Sema3e-HTVi liver treated with CCl_4 had markedly disoriented and contracted SECs, whereas radial arrays of SECs were reconstructed around the CV in control-HTVi liver (Figure 3E), which was similar to the image 24 hours after CCl_4 treatment (Figure 1D and Supplemental Figure S1D). Consistent with this observation, the vascular system of the Sema3e-HTVi liver decreased significantly compared with that of the control-HTVi liver (Figure 3F). These results suggest that Sema3e is able to affect the morphologic status of SECs in regeneration process *in vivo* and *in vitro*.

Disoriented Sinusoidal Regeneration by Sema3e Potentiates HSC Activation *in Vivo*

We examined whether regeneration of hepatocytes was affected after liver injury because inhibiting sinusoidal reconstruction in Sema3e-HTVi liver may affect blood flow in the liver. However, no significant differences were observed between control- and Sema3e-HTVi livers after H&E staining (Figure 4A) or by serum albumin concentration (Supplemental Figure S5). We next investigated the status of HSCs, another key component of the liver sinusoid. Because HSCs express p75 low-affinity neurotrophic growth factor receptor (p75NTR),[28,29] SECs and HSCs in a regenerating sinusoid were visualized by IHC using anti—Stab-2 and anti-p75NTR antibodies. Normal sinusoids were reconstructed in control-HTVi liver 3 days after CCl_4 treatment (ie, each HSC-lined SEC was rearranged correctly). In contrast, many extended HSCs were observed accompanied by disorganized revascularization in the Sema3e-HTVi liver (Figure 4B). Moreover, most of these HSCs were not lined by SECs. HSCs and SECs are reciprocally regulated, and transient activation of HSCs is beneficial for wound healing during regeneration. Therefore, we supposed that the activation of HSCs was prolonged because of the lack of regulation by SECs. Actually, an expression analysis of α-smooth

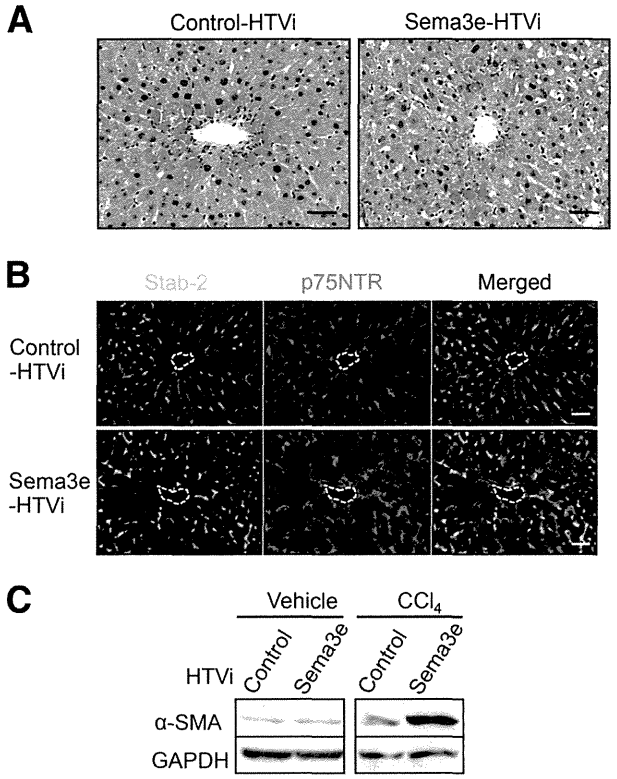

Figure 4 Disoriented sinusoidal regeneration by semaphorin 3E (Sema3e) potentiates hepatic stellate cell (HSC) activation *in vivo*. **A:** Hematoxylin and eosin staining of liver sections 3 days after carbon tetrachloride (CCl_4) treatment. No apparent difference is observed between control—hydrodynamic tail-vein injection (HTVi) and Sema3e-HTVi livers. **B:** Immunostaining of liver sections with anti—stabilin-2 (Stab-2) and anti-p75 low-affinity neurotrophic growth factor receptor (p75NTR) antibodies 3 days after CCl_4 treatment. Many HSCs in Sema3e-HTVi liver are not lined by sinusoidal endothelial cells (SECs) compared with that in control-HTVi liver. Broken line indicates central vein. **C:** Western blot analysis of α-smooth muscle actin (α-SMA) in liver 3 days after treatment with vehicle or CCl_4. α-SMA protein level in CCl_4-treated liver increases markedly in Sema3e-HTVi liver compared with the control, whereas the levels in vehicle-injected livers are not significantly different between Sema3e-HTVi and control-HTVi liver. Scale bar = 50 μm. GAPDH, glyceraldehyde-3-phosphate dehydrogenase.

muscle actin, an HSC activation marker, by Western blot analysis revealed activation of HSCs in Sema3e-HTVi liver compared with that in control-HTVi liver (Figure 4C). In contrast, the vehicle treatment did not activate the HSCs irrespective of continuous Sema3e expression, suggesting that Sema3e does not directly activate uninjured HSCs. Thus, Sema3e is likely to activate HSCs through SECs only when the sinusoid is undergoing reconstruction. These results suggest that transient expression of Sema3e by degenerating hepatocytes might contribute to the initial step of wound healing by activating HSCs.

Consecutive Expression of Sema3e Is a Risk Factor for Liver Fibrosis

Hepatocytes continue to be damaged in chronic hepatitis, and sinusoids are regenerated repeatedly. Given that continuous Sema3e expression resulted in activating HSCs, consecutive exposure of Sema3e under chronic hepatitis might contribute to the risk of fibrosis through prolonged HSC activation. We used *Sema3e*-KO mice to address this hypothesis. First, we compared hepatocellular damage induced by a single administration of CCl_4 between wild-type and *Sema3e*-KO mice. We found no significant difference in serum ALT level between both genotypes after CCl_4 administration (Supplemental Figure S6), suggesting that Sema3e deficiency does not directly affect the CCl_4-mediated hepatocellular cytotoxicity. Second, we evaluated the morphologic status of SECs and HSCs 24 hours after

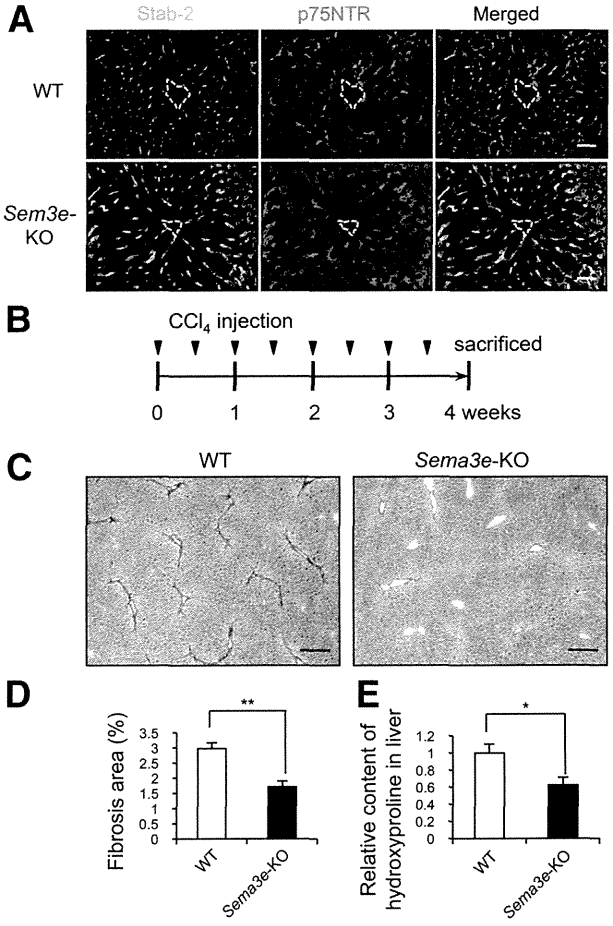

Figure 5 Lack of semaphorin 3E (Sema3e) affects sinusoidal regeneration and attenuates liver fibrosis. **A:** Immunostaining of liver sections with anti—stabilin-2 (Stab-2) and anti-p75 low-affinity neurotrophic growth factor receptor (p75NTR) antibodies 24 hours after carbon tetrachloride (CCl_4) treatment. **B:** Sinusoidal endothelial cell (SEC) morphologic status in wild-type (WT) mice is markedly contracted, whereas that of *Sema3e*-knockout (KO) mice is less affected. Broken line indicates central vein (CV). Experimental scheme for liver fibrogenesis in wild-type and *Sema3e*-KO mice. **C** and **D:** A total of 1.0 mL/kg of i.p. CCl_4 was injected into each mouse twice per week for 4 weeks, and then the liver was harvested. Sirius Red staining of liver sections after CCl_4 treatment. **E:** WT mouse liver exhibits marked accumulation of fibers around the CV, whereas the *Sema3e*-KO mouse liver appears less fibrotic. Relative hydroxyproline (Hp) content in liver. *Sema3e*-KO livers contain less Hp than WT livers. Data are expressed means ± SEM. $n = 5$ per group. $^*P < 0.05$, $^{**}P < 0.01$. Scale bars: 50 μm (**B**); 200 μm (**E**).

CCl_4 treatment in wild-type and *Sema3e*-KO mice. The SECs were markedly contracted in wild-type mice, whereas they were less affected in *Sema3e*-KO mice (Figure 5A). These results indicate that not only the robust expression of Sema3e but also the lack of Sema3e could affect sinusoidal regeneration. Moreover, almost all HSCs were associated with SECs in *Sema3e*-KO mice, but many HSCs were not lined by SECs in wild-type mice (Figure 5A). Finally, the morphologic features of both wild-type and *Sema3e*-KO SECs reverted to the original shape 72 hours after CCl_4 treatment (Supplemental Figure S7).

To further investigate the involvement of Sema3e in liver regeneration and fibrosis, chronic hepatitis was induced in wild-type and *Sema3e*-KO mice by repeated administration of CCl_4 (Figure 5B). We investigated the proliferation of hepatocytes 72 hours after the final CCl_4 injection by IHC using an anti–Ki-67 antibody. We found no significant differences in the rate of Ki-67–positive hepatocytes around the CV between wild-type and *Sema3e*-KO mice (Supplemental Figure S8, A and B). However, Picro Sirius Red staining revealed that the accumulation of collagen fibers was markedly decreased in *Sema3e*-KO mice compared with wild-type mice (Figure 5, C and D). Actually, the hydroxyproline content in liver, which reflects the amount of collagen, decreased significantly in *Sema3e*-KO mice compared with wild-type mice (Figure 5E), indicating that the lack of Sema3e attenuates liver fibrosis. In addition, *Sema3e*-KO SECs around the CV exhibited a more extended morphologic status than wild-type SECs even after chronic injury (Supplemental Figure S9). These results indicate that continuous exposure to Sema3e under a chronic hepatitis condition contributes to the exacerbation of liver fibrosis.

Discussion

We found that Sema3e plays significant roles in sinusoidal regeneration and the progression of liver fibrosis (Figure 6). We found that damaged hepatocytes transiently expressed Sema3e, which induced contraction of SECs in CCl_4-mediated liver injury model. Because free radical derived from CCl_4 metabolite damages the liver cells, we cannot exclude the possibility that cytotoxicity or cellular alterations due to proteolysis may partly contribute to the thinner staining of SECs by IHC. However, the staining patterns by two distinct SEC surface markers, Stab-2 and FcγR, exhibited a similar contracted morphologic status. In addition, *Sema3e*-KO SECs were less contracted than wild-type SECs after CCl_4 administration despite no significant differences in hepatocellular cytotoxicity, strongly suggesting that contraction of SEC was caused by Sema3e actively rather than passive cellular alterations.

Various functions of semaphorins and their receptors have been revealed recently. Among them, regulation of angiogenesis as a repulsive cue is a well-known function of type 3 semaphorins. In particular, Sema3e inhibits extension of endothelial tip cells that play a significant role in angiogenic guidance. In contrast, Sema3e and Plxnd1 are expressed in macrophages of advanced atherosclerotic plaques and regulate their retention.[26] However, the functional significance of Sema3e in liver disease remains unknown. Because Sema3e and Plxnd1 mRNA were not detected in CD45-positive blood cells, including macrophages in either normal or CCl_4-treated liver, it is unlikely that blood cells are related to a series of SEC morphologic changes directly. Meanwhile, Sema3e expression was induced in damaged hepatocytes. Although the signaling pathway implicated in Sema3e expression is largely unknown, Moriya et al[30] found that p53 expression up-regulated Sema3e expression in HUVEC and ischemic limb. Considering that reactive oxygen species (ROS) relate to the activation of p53 signaling,[31] drastic expression of Sema3e in CCl_4-injured liver may be promoted in a p53-dependent manner. In addition, the modest induction of Sema3e in primary cultured hepatocytes without ROS suggests the possibility that a cellular stress by dissociation or culture is involved in Sema3e expression. In fact, we have observed that the other hepatitis models, such as concanavalin-A injection or 3,5-diethoxycarbonyl-1,4-dihydrocollidine feeding, also induce potent expression of Sema3e (data not shown), suggesting the existence of another pathway independent of ROS stimuli. Further studies are needed to elucidate alternative signaling pathways.

Secreted type 3 semaphorins have been considered to function in an autocrine manner during angiogenesis. However, our findings indicate that Sema3e may play a

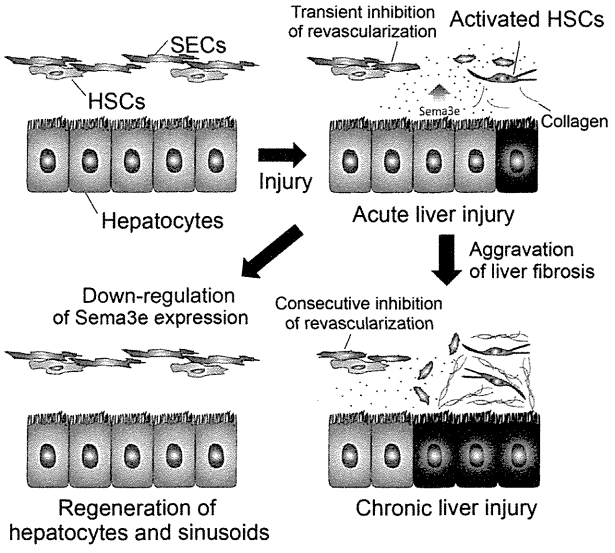

Figure 6 A model of the regulatory mechanism of sinusoidal regeneration and liver fibrosis by semaphorin 3E (Sema3e) signaling. Damaged hepatocytes express Sema3e transiently to promote contraction of sinusoidal endothelial cells (SECs), which diminishes the influence by hepatic stellate cells (HSCs). Consequently, isolated HSCs are more easily activated to promote liver regeneration during wound healing. However, consecutive Sema3e expression during chronic liver injury causes sustained inhibition of sinusoidal regeneration and HSC activation, resulting in collagen accumulation.

significant role not only in the regulation of sinusoidal regeneration but also in fibrogenesis through HSCs in a paracrine manner. The Sema3e/Plxnd1 axis counteracts VEGF/VEGFR-2 signaling via a feedback mechanism.[19] Because selective activation of VEGFR-1 on SECs stimulates hepatocyte proliferation *in vivo* and reduces liver damage in mice exposed to CCl_4,[32] transient expression of Sema3e may contribute to liver regeneration by skewing VEGFR-2 signaling to VEGFR-1. Alternatively, considering that the activation of SECs and/or HSCs contributes to the proliferation of hepatocytes by producing mitogenic cytokines, the regeneration of hepatocytes may be aberrant in *Sema3e*-KO mice. Although no significant difference was found in hepatocyte proliferation between wild-type and *Sema3e*-KO mice after chronic liver injury, further investigation will be required to make a conclusion.

In terms of physiologic significance of transient Sema3e expression by damaged hepatocytes, its possible role in wound repair will be taken into account. The recruitment of immune cells to a damaged site is a step for wound healing.[33] Macrophages operate as voracious phagocytes, clearing the wound of all matrix and cell debris. Therefore, enhanced permeability and decreased density of sinusoids by Sema3e could contribute to wound repair by facilitating the migration of immune cells to damaged region.

Because a massive volume of blood flows into the liver sinusoids, a fine balance between proangiogenic and antiangiogenic signaling is required for liver homeostasis. For example, VEGF, the primary proangiogenic factor in sinusoidal regeneration, is transiently up-regulated after liver injury.[34] However, constitutive expression of VEGF, which is induced by chronic liver injury, results in aberrant angiogenesis and the development of abnormal vascular architecture that is strongly linked to progressive fibrogenesis.[35] Thus, disrupting the balance leads directly to pathologic changes. Therefore, transient expression of Sema3e by damaged hepatocytes may contribute to the fine-tuning of sinusoidal regeneration and the inhibition of aberrant angiogenesis. Taken together, our results suggest that Sema3e contributes to the initial steps of liver regeneration by providing a scaffold for proliferating hepatocytes through activating HSCs. In addition, progressive fibrogenesis could be caused not only by consecutive expression of a proangiogenic factor but also by an antiangiogenic factor. In conclusion, our findings indicate that Sema3e is the main antiangiogenic player of SECs during liver injury and that consecutive Sema3e expression is a risk factor for liver fibrosis. These results suggest that Sema3e or Plxnd1 could be a therapeutic target in liver fibrosis and cirrhosis.

Acknowledgments

We thank Dr. Yutaka Yoshida and Dr. Atsushi Kumanogoh for providing *Sema3e*-KO mice, Naoko Miyata for assistance with flow cytometry, Yoshiko Kamiya for mouse and technical assistance, and the members of the Miyajima laboratory for helpful discussion and suggestions.

Supplemental Data

Supplemental material for this article can be found at *http://dx.doi.org/10.1016/j.ajpath.2014.04.018*.

References

1. Taub R: Liver regeneration: from myth to mechanism. Nat Rev Mol Cell Biol 2004, 5:836–847
2. Selden AC, Hodgson HJ: Growth factors and the liver. Gut 1991, 32: 601–603
3. Michalopoulos GK, DeFrances MC: Liver regeneration. Science 1997, 276:60–66
4. Raghow R: The role of extracellular matrix in postinflammatory wound healing and fibrosis. FASEB J 1994, 8:823–831
5. Zhang DY, Friedman SL: Fibrosis-dependent mechanisms of hepatocarcinogenesis. Hepatology 2012, 56:769–775
6. Friedman SL, Roll FJ, Boyles J, Bissell DM: Hepatic lipocytes: the principal collagen-producing cells of normal rat liver. Proc Natl Acad Sci U S A 1985, 82:8681–8685
7. DeLeve LD, Wang X, Hu L, McCuskey MK, McCuskey RS: Rat liver sinusoidal endothelial cell phenotype is maintained by paracrine and autocrine regulation. Am J Physiol Gastrointest Liver Physiol 2004, 287:G757–G763
8. Deleve LD, Wang X, Guo Y: Sinusoidal endothelial cells prevent rat stellate cell activation and promote reversion to quiescence. Hepatology 2008, 48:920–930
9. Tanaka H, Leung PS, Kenny TP, Gershwin ME, Bowlus CL: Immunological orchestration of liver fibrosis. Clin Rev Allergy Immunol 2012, 43:220–229
10. Nishina T, Komazawa-Sakon S, Yanaka S, Piao X, Zheng DM, Piao JH, Kojima Y, Yamashina S, Sano E, Putoczki T, Doi T, Ueno T, Ezaki J, Ushio H, Ernst M, Tsumoto K, Okumura K, Nakano H: Interleukin-11 links oxidative stress and compensatory proliferation. Sci Signal 2012, 5:ra5
11. Li F, Huang Q, Chen J, Peng Y, Roop DR, Bedford JS, Li CY: Apoptotic cells activate the "phoenix rising" pathway to promote wound healing and tissue regeneration. Sci Signal 2010, 3:ra13
12. Okabe M, Tsukahara Y, Tanaka M, Suzuki K, Saito S, Kamiya Y, Tsujimura T, Nakamura K, Miyajima A: Potential hepatic stem cells reside in EpCAM+ cells of normal and injured mouse liver. Development 2009, 136:1951–1960
13. Inagaki FF, Tanaka M, Inagaki NF, Yagai T, Sato Y, Sekiguchi K, Oyaizu N, Kokudo N, Miyajima A: Nephronectin is upregulated in acute and chronic hepatitis and aggravates liver injury by recruiting CD4 positive cells. Biochem Biophys Res Commun 2013, 430: 751–756
14. Yazdani U, Terman JR: The semaphorins. Genome Biol 2006, 7:211
15. Zhou Y, Gunput RA, Pasterkamp RJ: Semaphorin signaling: progress made and promises ahead. Trends Biochem Sci 2008, 33:161–170
16. Gu C, Giraudo E: The role of semaphorins and their receptors in vascular development and cancer. Exp Cell Res 2013, 319:1306–1316
17. Gu C, Yoshida Y, Livet J, Reimert DV, Mann F, Merte J, Henderson CE, Jessell TM, Kolodkin AL, Ginty DD: Semaphorin 3E and plexin-D1 control vascular pattern independently of neuropilins. Science 2005, 307:265–268
18. Sakurai A, Gavard J, Annas-Linhares Y, Basile JR, Amornphimoltham P, Palmby TR, Yagi H, Zhang F, Randazzo PA, Li X, Weigert R, Gutkind JS: Semaphorin 3E initiates antiangiogenic signaling through plexin D1 by regulating Arf6 and R-Ras. Mol Cell Biol 2010, 30:3086–3098

19. Kim J, Oh WJ, Gaiano N, Yoshida Y, Gu C: Semaphorin 3E-Plexin-D1 signaling regulates VEGF function in developmental angiogenesis via a feedback mechanism. Genes Dev 2011, 25:1399–1411
20. Nonaka H, Tanaka M, Suzuki K, Miyajima A: Development of murine hepatic sinusoidal endothelial cells characterized by the expression of hyaluronan receptors. Dev Dyn 2007, 236:2258–2267
21. Takase HM, Itoh T, Ino S, Wang T, Koji T, Akira S, Takikawa Y, Miyajima A: FGF7 is a functional niche signal required for stimulation of adult liver progenitor cells that support liver regeneration. Genes Dev 2013, 27:169–181
22. Miyaoka Y, Ebato K, Kato H, Arakawa S, Shimizu S, Miyajima A: Hypertrophy and unconventional cell division of hepatocytes underlie liver regeneration. Curr Biol 2012, 22:1166–1175
23. Reddy GK, Enwemeka CS: A simplified method for the analysis of hydroxyproline in biological tissues. Clin Biochem 1996, 29:225–229
24. Nonaka H, Sugano S, Miyajima A: Serial analysis of gene expression in sinusoidal endothelial cells from normal and injured mouse liver. Biochem Biophys Res Commun 2004, 324:15–24
25. Weddle CC, Hornbrook KR, McCay PB: Lipid peroxidation and alteration of membrane lipids in isolated hepatocytes exposed to carbon tetrachloride. J Biol Chem 1976, 251:4973–4978
26. Wanschel A, Seibert T, Hewing B, Ramkhelawon B, Ray TD, van Gils JM, Rayner KJ, Feig JE, O'Brien ER, Fisher EA, Moore KJ: Neuroimmune guidance cue Semaphorin 3E is expressed in atherosclerotic plaques and regulates macrophage retention. Arterioscler Thromb Vasc Biol 2013, 33:886–893
27. Fukushima Y, Okada M, Kataoka H, Hirashima M, Yoshida Y, Mann F, Gomi F, Nishida K, Nishikawa S, Uemura A: Sema3E-PlexinD1 signaling selectively suppresses disoriented angiogenesis in ischemic retinopathy in mice. J Clin Invest 2011, 121:1974–1985
28. Suzuki K, Tanaka M, Watanabe N, Saito S, Nonaka H, Miyajima A: p75 Neurotrophin receptor is a marker for precursors of stellate cells and portal fibroblasts in mouse fetal liver. Gastroenterology 2008, 135:270–281.e273
29. Passino MA, Adams RA, Sikorski SL, Akassoglou K: Regulation of hepatic stellate cell differentiation by the neurotrophin receptor p75NTR. Science 2007, 315:1853–1856
30. Moriya J, Minamino T, Tateno K, Okada S, Uemura A, Shimizu I, Yokoyama M, Nojima A, Okada M, Koga H, Komuro I: Inhibition of semaphorin as a novel strategy for therapeutic angiogenesis. Circ Res 2010, 106:391–398
31. Liu B, Chen Y, St Clair DK: ROS and p53: a versatile partnership. Free Radic Biol Med 2008, 44:1529–1535
32. LeCouter J, Moritz DR, Li B, Phillips GL, Liang XH, Gerber HP, Hillan KJ, Ferrara N: Angiogenesis-independent endothelial protection of liver: role of VEGFR-1. Science 2003, 299:890–893
33. Martin P, Leibovich SJ: Inflammatory cells during wound repair: the good, the bad and the ugly. Trends Cell Biol 2005, 15:599–607
34. Ishikawa K, Mochida S, Mashiba S, Inao M, Matsui A, Ikeda H, Ohno A, Shibuya M, Fujiwara K: Expressions of vascular endothelial growth factor in nonparenchymal as well as parenchymal cells in rat liver after necrosis. Biochem Biophys Res Commun 1999, 254:587–593
35. Valfre di Bonzo L, Novo E, Cannito S, Busletta C, Paternostro C, Povero D, Parola M: Angiogenesis and liver fibrogenesis. Histol Histopathol 2009, 24:1323–1341

 DOI: 10.1002/eji.201444570 Eur. J. Immunol. 2014. 44: 2638–2647

European Journal of Immunology

Mature resting Ly6C^{high} natural killer cells can be reactivated by IL-15

Ai Omi, Yutaka Enomoto, Tsuyoshi Kiniwa, Naoko Miyata and Atsushi Miyajima

Laboratory of Cell Growth and Differentiation, Institute of Molecular and Cellular Biosciences, University of Tokyo, Tokyo, Japan

Mature NK cells are heterogeneous as to their expression levels of cell surface molecules. However, the functional differences and physiological roles of each NK-cell subset are not fully understood. In this study, we report that based on the Ly6C expression levels, mature C57BL/6 murine NK cells can be subdivided into Ly6C^{low} and Ly6C^{high} subsets. Ly6C^{high} NK cells are in an inert state as evidenced by the production of lower levels of IFN-γ and granzyme B, and they exhibit poorer proliferative potential than Ly6C^{low} NK cells. In addition, adoptive transfer experiments revealed that Ly6C^{high} NK cells are derived from Ly6C^{low} NK cells in the steady state. These results strongly suggest that Ly6C^{high} NK cells are resting cells in the steady state. However, in vitro, Ly6C^{high} NK cells become Ly6C^{low} NK cells with strong effector functions upon stimulation with IL-15. Moreover, Ly6C^{high} NK cells also revert to Ly6C^{low} NK cells in vivo upon injection of the IL-15 inducers polyI:C and CpG. Taken together, these results demonstrate the plasticity of mature NK cells and suggest that Ly6C^{high} NK cells are a reservoir of potential NK cells that allow effective and strong response to infections.

Keywords: Innate immunity · Interleukin · Memory · NK cell · Viral infection

Additional supporting information may be found in the online version of this article at the publisher's web-site

Introduction

NK cells are the third most populous lymphocytes and contribute to innate immune responses as effector cells [1, 2]. NK cells are distributed throughout the body, in both lymphoid and nonlymphoid organs, for participation in immune surveillance of tumors or viral infection [1, 3, 4]. Among their various functions, NK cells play major roles in cytotoxicity and the production of inflammatory cytokines such as IFN-γ [1, 3, 4]. Unlike B and T lymphocytes, NK cells do not express a rearranged Ag-specific receptor, but express many types of activating and inhibitory receptors that recognize target cells [2–4]. Cross-linking of these receptors by their ligands regulates the functions of NK cells, and activated NK cells secrete large amounts of IFN-γ and cytotoxic granules containing perforin and granzyme B [1, 3]. Given these features, NK cells have been classified as group 1 innate lymphoid cells [5].

NK cells are differentiated from hematopoietic stem cells and develop in mainly the BM [6]. In mice, NK-cell progenitors express CD122, which is the common subunit of IL-2R and IL-15R [6]. NK cells in the early developmental stage express NK1.1 and NKG2D, followed by the expression of inhibitory and activating receptors such as those in the CD94-NKG2 family or LY49 family [6]. Thereafter, NK cells in the late developmental stage express CD11b at high levels and become mature NK cells [6]. Thus, NK cells show different expression patterns of these surface markers during development and maturation.

Mature NK cells were originally described as a homogenous cell population characterized by their ability to mediate spontaneous

Correspondence: Dr. Yutaka Enomoto
e-mail: yenomoto@iam.u-tokyo.ac.jp

cytotoxicity against target cells [7–9]. However, in the early 1980s it was proposed that human mature NK cells in peripheral blood can be subdivided into two functional subsets based on the expression of CD56 [10]. $CD56^{dim}$ and $CD56^{bright}$ NK cells exhibit clearly distinct effector functions; that is, $CD56^{dim}$ NK cells posess high cytotoxic capacity, while $CD56^{bright}$ NK cells produce a large amount of cytokines [11–13]. However, as CD56 is not expressed in mice, it has been difficult to identify functionally distinct NK-cell subsets in mice. Recently, efforts have been made to find cell surface markers that can be used to characterize mature murine NK cells and several candidate molecules such as CD27, KLRG1, and CD94 have been found. These studies revealed that mature murine NK cells can be also subdivided into subsets [14–16]. However, their functional differences and physiological roles of each subset remain elusive.

To address this question, we searched for a better marker that can be used to characterize mature NK cells. In the present study, we report that mature murine NK cells ($NK1.1^+CD11b^+CD3e^-$) can be subdivided according to their Ly6C expression levels into $Ly6C^{low}$ and $Ly6C^{high}$ subsets. Ly6C is a member of the Ly6 superfamily and is a glycosylphosphatidylinositol-anchored cell surface molecule [17]. Ly6C is expressed mainly in lymphocytes, monocytes/macrophages, granulocytes, and endothelial cells, and is a useful marker to distinguish the various developmental stages of these cells [18–20]. Moreover, it is well known that memory $CD8^+$ T cells as well as activated $CD8^+$ T cells express higher levels of Ly6C than naive cells [2, 20, 21]. Therefore, Ly6C is often used as a maker of activation and memory in T cells. Both NK cells and $CD8^+$ T cells are derived from a common lymphoid progenitor, and have many common features [2, 22]. However, the characteristics of $Ly6C^{low}$ and $Ly6C^{high}$ NK-cell subsets are not fully understood [23]. We found that there are two states in mature murine NK cells; that is, $Ly6C^{low}$ NK cells are active state and $Ly6C^{high}$ NK cells are resting, respectively. Furthermore, we herein describe the plasticity of mature NK cells.

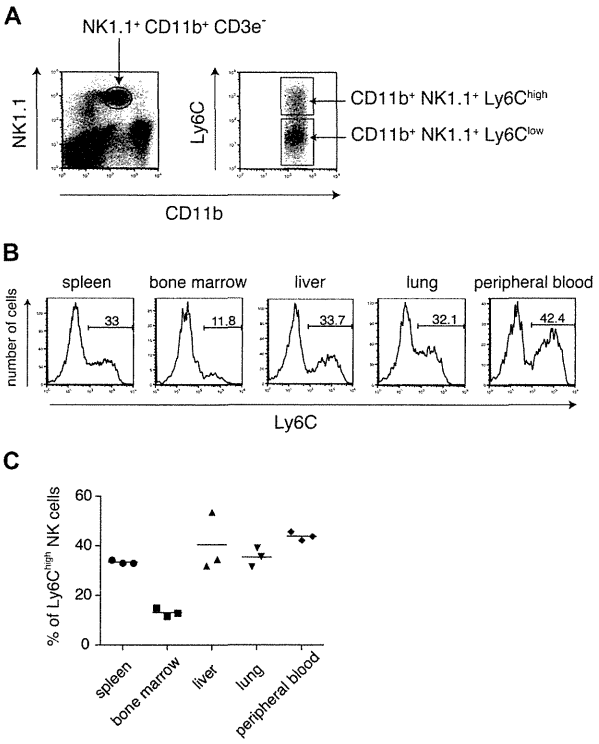

Figure 1. Ly6C expression on mature murine NK cells. (A) Cells were isolated from the spleen of C57BL/6 mice and Ly6C expression was assessed by flow cytometry. The dot plots of the right panel were gated on $NK1.1^+CD11b^+CD3e^-$ cells. (B) Cells were isolated from the spleen, BM, liver, lung, and peripheral blood of C57BL/6 mice and Ly6C expression was determined by flow cytometry, gating on $NK1.1^+CD11b^+CD3e^-$ cells. (C) The percentages of $Ly6C^{high}$ NK cells, as determined in (B), in each tissue are shown. Each symbol represents an individual mouse and bars represent the means within the groups ($n = 3$). p-value was calculated with one-way ANOVA method followed by Tukey's studentized range test to elucidate the group differences. BM versus spleen, liver, lung, peripheral blood: $p < 0.01$. (A and B) Data shown are from a single experiment representative of three independent experiments performed.

Results

Surface expression of Ly6C defines two subsets of mature murine NK cells

We found that mature murine NK cells ($NK1.1^+CD11b^+CD3e^-$) in the spleen can be subdivided into two populations based on the expression levels of Ly6C (Fig. 1A and B). Immature NK cells ($NK1.1^+CD11b^-CD3e^-CD27^+$) [24] were also subdivided by the expression of Ly6C, though the population of Ly6C-expressing cells was very small (Supporting Information Fig. 1).

To reveal the tissue distribution of the $Ly6C^{low}$ and $Ly6C^{high}$ subsets in mature NK cells in vivo, we examined the abundance of each NK-cell subset in lymphoid and nonlymphoid organs, such as the spleen, BM, liver, lung, and peripheral blood by flow cytometry (Fig. 1B). Although both $Ly6C^{low}$ and $Ly6C^{high}$ NK-cell subsets were found in various peripheral tissues, a majority of NK cells in the BM, in which NK cells develop [6], expressed Ly6C at low levels (Fig. 1B and C). These results indicate that the $Ly6C^{high}$ NK-cell subset is present mainly in peripheral tissues.

Distinct expression patterns of surface markers in NK-cell subsets

NK cells express various activating and inhibitory receptors, and their expression patterns are closely coupled to NK-cell functions [2–4]. Thus, we examined the surface expression of NK-cell receptors on $Ly6C^{low}$ and $Ly6C^{high}$ NK cells by flow cytometry (Fig. 2A and B). The expression levels of activating receptors were similar between $Ly6C^{low}$ and $Ly6C^{high}$ NK-cell subsets with the exception of Ly49H (Fig. 2A). In contrast, $Ly6C^{high}$ NK cells displayed higher proportions of cells expressing the inhibitory receptors KLRG1 and Ly49C/I than did $Ly6C^{low}$ NK cells (Fig. 2B). Conversely, the Ly49A expression levels of $Ly6C^{low}$ NK cells were slightly higher than those of $Ly6C^{high}$ NK cells (Fig. 2B). Furthermore, we investigated

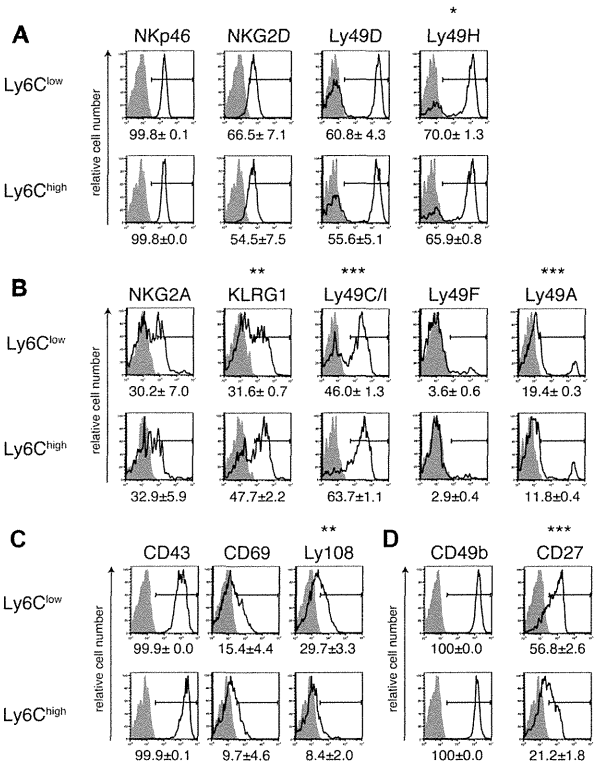

Figure 2. Characterization of surface markers on Ly6C^{low} and Ly6C^{high} NK-cell subsets. (A–D) Cells isolated from the spleens of C57BL/6 mice were stained for the indicated cell surface markers. Ly6C^{low} and Ly6C^{high} NK-cell subsets were gated on NK1.1$^+$CD11b$^+$CD3e$^-$ cells. Shaded histograms indicate isotype control. The numbers under each histogram show the mean (±SEM) percentages of positive cells for surface marker expression calculated from three mice and the histograms are representative of three independent experiments performed. *$p < 0.05$, **$p < 0.01$, ***$p < 0.001$ (Student's two-tailed t-test).

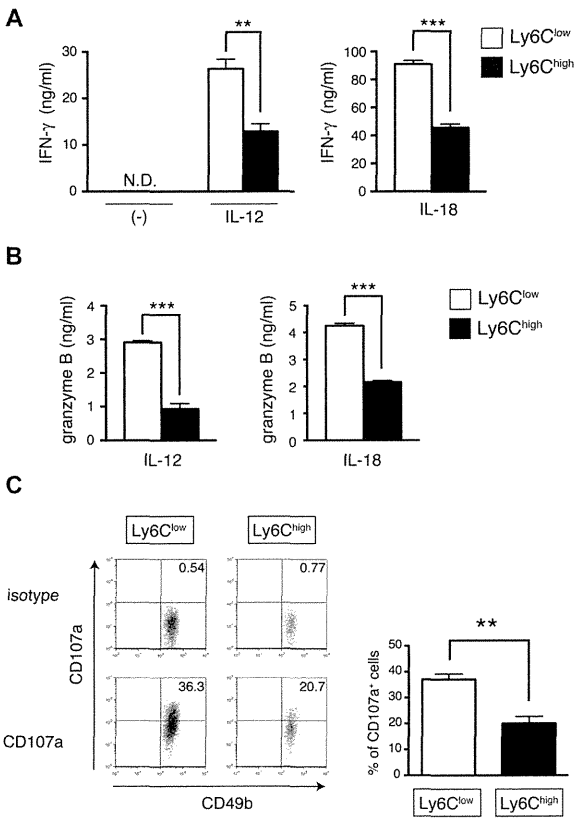

Figure 3. IFN-γ production and granzyme B secretion of Ly6C^{low} NK cells and Ly6C^{high} NK cells. (A and B) CD49b$^+$CD11b$^+$CD3e$^-$Ly6C^{low} NK cells and CD49b$^+$CD11b$^+$CD3e$^-$ Ly6C^{high} NK cells were sorted from the spleens of C57BL/6 mice. Sorted NK-cell subsets (5×10^4 cells/well) were stimulated with IL-12 (100 ng/mL) or IL-18 (100 ng/mL) in the presence of IL-2 (100 ng/mL). After 24 h of incubation, the levels of (A) IFN-γ and (B) granzyme B in the culture supernatants were measured by ELISA. Data are shown as means + SEM of three samples. (C) CD49b$^+$ NK cells were cultured with IL-18 (100 ng/mL) in the presence of IL-2 (100 ng/mL). After 16 h of incubation, NK cells were cocultured with YAC-1 cells by an E:T ratio of 1:1. The dot plot represents the percentage of CD107a$^+$ cells gated on CD49b$^+$CD11b$^+$CD3e$^-$ Ly6C^{low} or Ly6C^{high} NK cells. The bar graphs represent the means (+SEM) percentages of CD107a$^+$ cells ($n = 3$). All data shown are from a single experiment representative of three independent experiments performed. **$p < 0.01$, ***$p < 0.001$. N.D., not detected (Student's two-tailed t-test).

activation markers known to be upregulated in activated NK cells [25–28] and found that the expression levels of Ly108 were significantly lower in Ly6C^{high} NK cells than in Ly6C^{low} NK cells (Fig. 2C). Taken together, these results suggest that the activity of Ly6C^{high} NK cells is lower than that of Ly6C^{low} NK cells. We next examined the expression of maturation markers in NK cells, namely CD49b and CD27 [6, 14, 24]. CD49b was highly expressed in both Ly6C^{low} and Ly6C^{high} NK cells (Fig. 2D), whereas Ly6C^{high} NK cells displayed lower proportions of cells expressing CD27 than did Ly6C^{low} NK cells (Fig. 2D). This result implies that the maturation stage of Ly6C^{low}and that of Ly6C^{high} NK cells are different. While it has been known that CD27 subdivides mature murine NK cells into two populations, our results suggest that the expression of Ly6C did not match the expression of CD27 completely.

Ly6C^{high} cells are inert NK cells

NK cells have various functions in the immune system. Among them, IFN-γ production and cytotoxicity play major roles for the clearance of infectious pathogens and tumor cells [1, 3, 4]. Therefore, we next examined IFN-γ production by each NK-cell subset. NK cells are known to produce IFN-γ in response to IL-12 or IL-18, which are secreted by APCs such as DCs [1, 29]. As shown in Figure 3A, both NK-cell subsets secreted IFN-γ in response to IL-12 or IL-18. However, IFN-γ secretion by Ly6C^{high} NK cells was approximately half that of Ly6C^{low} NK cells (Fig. 3A). In order to exclude the possibility that viability of NK-cell subsets were different during the assay, IL-2 was added to maintain the survival of NK cells [30, 31]. Subsequently, there was no difference in cell viability between Ly6C^{low} and ly6C^{high} NK cells (data not shown). Activated NK cells release cytotoxic granules containing perforin and granzyme B to kill target cells [1, 3]. Granzyme